Title

Uncoupling interferon signaling and antigen presentation to overcome immunotherapy resistance due to JAK1 loss in melanoma

Journal

Science Translational Medicine, 12(565)

ISSN

1946-6234

Authors

Kalbasi, Anusha

Tariveranmoshabad, Mito

Hakimi, Kevin

et al.

Publication Date

2020-10-14

DOI

10.1126/scitranslmed.abb0152

Peer reviewed

CANCER

Uncoupling interferon signaling and antigen presentation to overcome immunotherapy resistance due to JAK1 loss in melanoma

Anusha Kalbasi[1,2,3]*, Mito Tariveranmoshabad[1†], Kevin Hakimi[1†], Sarah Kremer[1], Katie M. Campbell[4], Juan M. Funes[2], Agustin Vega-Crespo[4], Giulia Parisi[4], Ameya Champekar[4], Christine Nguyen[1], Davis Torrejon[4], Daniel Shin[4], Jesse M. Zaretsky[4], Robert D. Damoiseaux[3,5,6], Daniel E. Speiser[7], Pedro P. Lopez-Casas[8], Marisol Quintero[8], Antoni Ribas[2,3,4,5,9]

Defects in tumor-intrinsic interferon (IFN) signaling result in failure of immune checkpoint blockade (ICB) against cancer, but these tumors may still maintain sensitivity to T cell–based adoptive cell therapy (ACT). We generated models of IFN signaling defects in B16 murine melanoma observed in patients with acquired resistance to ICB. Tumors lacking *Jak1* or *Jak2* did not respond to ICB, whereas ACT was effective against *Jak2*^{KO} tumors, but not *Jak1*^{KO} tumors, where both type I and II tumor IFN signaling were defective. This was a direct result of low baseline class I major histocompatibility complex (MHC I) expression in B16 and the dependency of MHC I expression on either type I or type II IFN signaling. We used genetic and pharmacologic approaches to uncouple this dependency and restore MHC I expression. Through independent mechanisms, overexpression of NLRC5 (nucleotide-binding oligomerization domain-like receptor family caspase recruitment domain containing 5) and intratumoral delivery of BO-112, a potent nanoplexed version of polyinosinic:polycytidylic acid (poly I:C), each restored the efficacy of ACT against B16-*Jak1*^{KO} tumors. BO-112 activated double-stranded RNA (dsRNA) sensing (via protein kinase R and Toll-like receptor 3) and induced MHC I expression via nuclear factor κB, independent of both IFN signaling and NLRC5. In summary, we demonstrated that in the absence of tumor IFN signaling, MHC I expression is essential and sufficient for the efficacy of ACT. For tumors lacking MHC I expression due to deficient IFN signaling, activation of dsRNA sensors by BO-112 affords an alternative approach to restore the efficacy of ACT.

INTRODUCTION

Intact tumor cell interferon (IFN) signaling was first identified as a critical piece of immune surveillance more than two decades ago (*1*, *2*). More recently, experience with immune checkpoint blockade (ICB) has validated the importance of tumor cell–intrinsic IFN signaling to antitumor immune responses in patients (*3*, *4*). Genetic or epigenetic disruption of tumor IFN signaling can result in primary or acquired resistance to ICB (*5*–*8*).

In primary resistance to ICB, tumor cell defects in IFN signaling disrupt adaptive expression of PD-L1 and negate the effects of targeting the PD-1/PD-L1 axis (*9*). In acquired resistance, defects in IFN signaling render tumor cells insensitive to the positive effects of IFNs on antigen presentation and chemoattractant expression and the negative effects of IFNs on cell proliferation. However, whether intact tumor IFN signaling regulates the direct cytotoxic capacity of a tumor-specific T cell is less clear. Upon engaging their target through recognition of the major histocompatibility complex (MHC)–antigen complex, tumor-specific T cells release granzyme and perforin, which induce apoptosis of the target cell (*10*). The role of tumor-intrinsic IFN signaling in this context is particularly relevant for adoptive cell therapy (ACT) approaches using tumor-specific T cells, such as T cell receptor (TCR)– or chimeric antigen receptor (CAR)–engineered T cell therapy.

To study the impact of tumor-intrinsic IFN signaling on the direct antitumor efficacy of tumor-specific T cells, we performed in vitro and adoptive transfer studies using tumor-specific T cells against a murine model of melanoma with IFN signaling defects (*Jak1* or *Jak2* loss) observed in patients with acquired resistance to ICB. Only defects in *Jak1* in which both type I and II tumor IFN signaling are disrupted negated the efficacy of adoptively transferred tumor-specific T cells, a by-product of the dependency of MHC I expression on either type I or type II IFN signaling. This dependency could be circumvented genetically by overexpressing NLRC5 (nucleotide-binding oligomerization domain-like receptor family caspase recruitment domain containing 5), which up-regulates MHC I independent of an IFN signal (*11*, *12*). As a pharmacologic approach, we used BO-112, a phase 1–tested, nanoplexed formulation of polyinosinic:polycytidylic acid (poly I:C) with activity in combination with ICB against tumors refractory to ICB monotherapy (*13*). BO-112 uncouples tumor IFN signaling and MHC I antigen presentation through activation of double-stranded RNA (dsRNA) sensing and nuclear factor κB (NF-κB) signaling, thereby restoring the efficacy of tumor-specific T cells.

RESULTS

B16-Jak1^{KO} tumors are resistant to ACT due to deficiency in both type I and II IFN signaling

To model the IFN signaling defects observed in human melanoma patients with primary or acquired resistance to ICB, we generated

[1]Department of Radiation Oncology, University of California Los Angeles (UCLA), Los Angeles, CA 90095, USA. [2]Division of Surgical Oncology, Department of Surgery, UCLA, Los Angeles, CA 90095, USA. [3]Jonsson Comprehensive Cancer Center, UCLA, Los Angeles, CA 90095, USA. [4]Division of Hematology-Oncology, Department of Medicine, UCLA, Los Angeles, CA 90095, USA. [5]Department of Molecular and Medical Pharmacology, UCLA, Los Angeles, CA 90095, USA. [6]California NanoSystems Institute, UCLA, Los Angeles, CA 90095, USA. [7]Department of Oncology, University of Lausanne, 1015 Lausanne, Switzerland. [8]Highlight Therapeutics, Paterna 46980 (Valencia), Spain. [9]Parker Institute for Cancer Immunotherapy, San Francisco, CA 94129, USA.
*Corresponding author. Email: anushakalbasi@mednet.ucla.edu
†These authors contributed equally to this work.

Jak1^{KO} and *Jak2*^{KO} B16-F10 cell lines using CRISPR. As a functional validation of the CRISPR knockout cell lines, surface PD-L1 expression was evaluated in response to type I (IFN-α and IFN-β) or type II (IFN-γ) IFNs (Fig. 1A). Consistent with their aberrant signaling, B16-*Jak2*^{KO} and B16-*Jak1*^{KO} tumors did not up-regulate surface PD-L1 in response to type II and either type I or II IFNs, respectively.

To evaluate the impact of defective tumor IFN signaling on response to ICB in the B16 model, we combined anti–PD-1 and anti–CTLA-4 checkpoint blockade with focal radiation therapy (XRT, 12 Gy) in a dual-flank tumor model, which results in a more robust antitumor immune response in the nonirradiated tumor than single or dual ICB (*14*, *15*). As expected, XRT and dual checkpoint blockade resulted

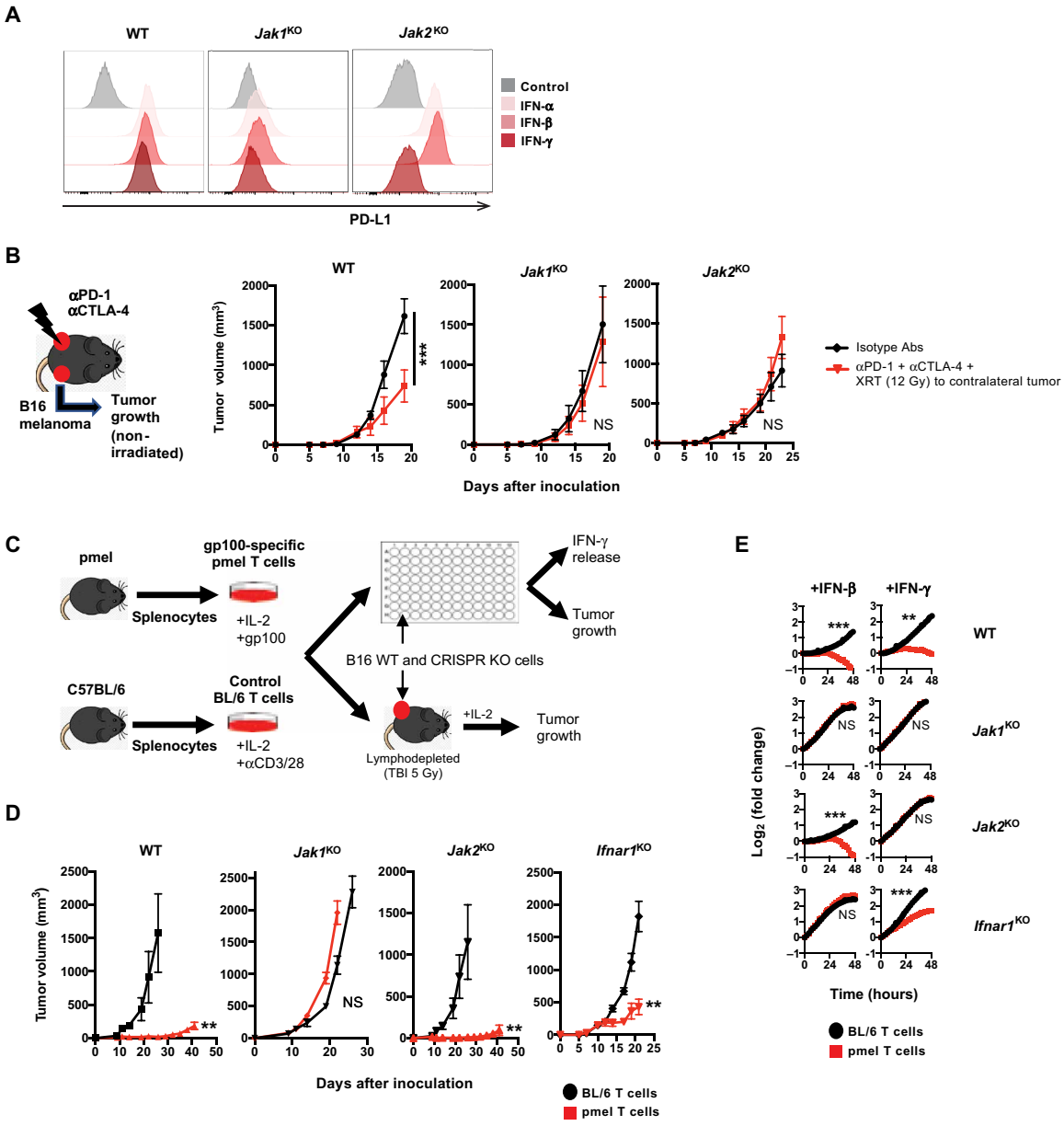

Fig. 1. *Jak1* loss, but not *Jak2 or Ifnar1* loss, mediates resistance of B16 melanoma to adoptively transferred tumor-specific T cells. (**A**) PD-L1 surface expression by flow cytometry in response to IFN-α, IFN-β, or IFN-γ. (**B**) Tumor growth (mean ± SEM) of nonirradiated tumors in a dual-flank model. Mice ($n = 4$ to 6 per group) were treated with focal tumor irradiation (12 Gy) to a contralateral tumor, along with αPD-1 and αCTLA-4 dual ICB (or relevant isotype controls); ***$P < 0.001$ (unpaired t test). NS, not significant; KO, knockout; Abs, antibodies; XRT, radiation therapy. (**C**) In vitro and in vivo modeling of efficacy of tumor-specific pmel T cells against B16 wild-type (WT) and CRISPR-modified cell line. (**D**) In vivo tumor growth (mean ± SEM) of CRISPR-modified B16-F10 tumors (WT, *Jak1*^{KO}, *Jak2*^{KO}, and *Ifnar1*^{KO}) after treatment with ACT. After lymphodepleting total body irradiation (TBI) (5 Gy), tumor-bearing mice ($n = 5$ per group) were treated with ACT consisting of one dose of 5.0×10^6 pmel (or control BL/6 T cells) along with IL-2 [50,000 IU/day intraperitoneally (i.p.) × 3 days]. **$P < 0.01$ (repeated-measures two-way ANOVA). (**E**) In vitro growth (mean ± SD) of CRISPR-modified B16-F10 tumor cell lines pretreated with either IFN-β (left) or IFN-γ (right) and cocultured with tumor-specific pmel T cells (red) or control BL/6 T cells (black). Cocultures performed in biological triplicate; error bars not visible as they are encompassed within the data points. **$P < 0.01$; ***$P < 0.001$(unpaired t test).

in a growth delay in the wild-type (WT) nonirradiated tumor ($P < 0.001$, multiple pairwise comparison); this effect was not observed in nonirradiated B16-*Jak2*^{KO} or B16-*Jak1*^{KO} tumors lacking type II IFN signaling or both type I and II IFN signaling, respectively (Fig. 1B). The absence of type II (*Jak2*^{KO}) IFN signaling or both (*Jak1*^{KO}) did not affect the antitumor effects on the irradiated tumor (fig. S1).

To test the sensitivity of IFN signaling–deficient tumors to tumor-specific T cells, we performed in vitro and adoptive transfer studies using T cells from pmel mice, which harbor a TCR transgene specific for gp100, a melanoma antigen highly expressed in B16 (Fig. 1C). B16 tumor cells retained gp100 expression after CRISPR modifications to IFN signaling pathways (fig. S2). Adoptive transfer of activated pmel T cells and interleukin-2 (IL-2) after lymphodepletion delayed the growth of WT tumors, compared to adoptive transfer of activated T cells from control C57BL/6 mice and IL-2 after lymphodepletion [$P < 0.01$, two-way analysis of variance (ANOVA); Fig. 1D]. Adoptively transferred pmel T cells retained antitumor efficacy against B16-*Jak2*^{KO} tumors deficient in type II IFN signaling. However, tumors lacking both type I and II IFN signaling (B16-*Jak1*^{KO}) were completely resistant to the antitumor effect of pmel T cells. To evaluate whether tumor-intrinsic type I IFN signaling alone was responsible for the resistance to pmel T cells, we generated B16-*Ifnar1*^{KO} tumors deficient in type I IFN signaling. Adoptively transferred pmel T cells retained efficacy against B16-*Ifnar1*^{KO} tumors.

We modeled these in vivo findings using an in vitro coculture system in which B16 WT or CRISPR-modified tumor cells were pretreated with either type I IFN-β or type II IFN-γ, and subsequently exposed to either control or pmel T cells. Pretreatment of WT B16 with either IFN-β or IFN-γ sensitized the tumor cells to killing by pmel T cells (Fig. 1E). Tumor cells pretreated with an IFN for which the cognate signaling pathway was defective (B16-*Jak2*^{KO} tumors pretreated with IFN-γ; B16-*Ifnar1*^{KO} tumors pretreated with IFN-β) were resistant to the cytotoxic effect of pmel T cells (Fig. 1E). B16-*Jak1*^{KO} tumor cells were resistant to killing by pmel T cells despite pretreatment with IFN-β or IFN-γ (Fig. 1E). On the basis of these data, we concluded that the in vivo sensitivity of B16 tumor cells to adoptively transferred pmel T cells is dependent on the activation of either type I or II IFN signaling. We hypothesized that this is related to the dependency of MHC I expression on either type I or II IFN signaling.

Human melanoma exhibits IFN-dependent expression of MHC I

IFN signaling is a well-described positive regulator of MHC I antigen-processing machinery (*16*). To better understand the role of IFN signaling in MHC I expression in melanoma, we evaluated the expression of MHC I in 48 human melanoma cell lines at baseline and in response to type I (IFN-α and IFN-β) and type II IFN (IFN-γ). Baseline MHC I expression in the human melanoma cell lines was distributed broadly, including a subset of cell lines with low baseline MHC I expression (Fig. 2A), similar to B16 murine melanoma (Fig. 1A). IFN-α, IFN-β, and IFN-γ augment the surface expression of MHC I ($P < 0.0001$); an absolute increase in MHC I expression was observed in 85% (41 of 48), 92% (44 of 48), and 79% (38 of 48) of cell lines, respectively (Fig. 2A and figs. S3 and S4). The relative increase in MHC I expression (mean fluorescence intensity, MFI) in response to IFN-γ was higher for cell lines in the lowest quartile of baseline MHC I expression, compared to the second, third, or fourth

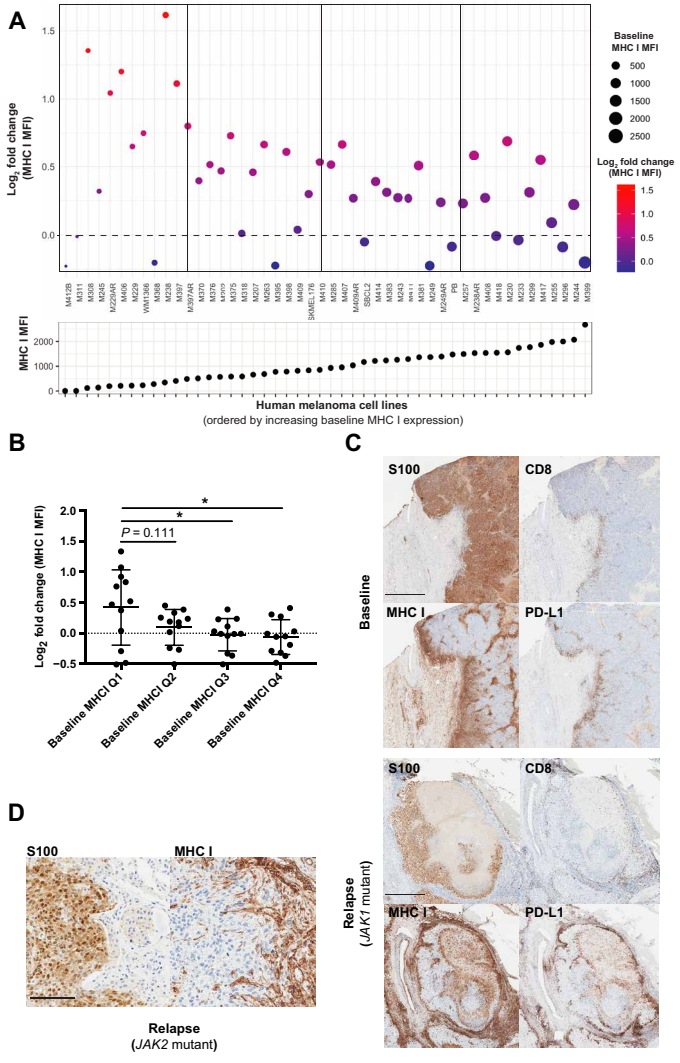

Fig. 2. MHC I expression of human melanoma exhibits IFN-γ dependence. (**A**) Effect of IFN-γ on surface MHC I expression of 48 human melanoma cell lines. Cell lines arranged from left to right by increasing MHC I expression (basal MHC I MFI shown in bottom panel and also as the diameter of the data point in the main panel). Data are shown as $\log_2$(fold change) of MFI of the IFN-γ–treated sample relative to untreated control [and also colored from blue to red according to value of $\log_2$(fold change)]. (**B**) Relative change in MFI (mean ± SD) upon IFN-γ exposure as related to basal MHC I expression. *$P < 0.05$ (unpaired *t* test). (**C**) Immunohistochemical staining analysis at baseline and at relapse in a patient with melanoma that developed acquired genetic resistance (loss-of-function *JAK1* mutation) to anti–PD-1 ICB. Scale bars, 1 mm (top) and 0.75 mm (bottom). (**D**) S100 (left) and MHC I (right) expression at the tumor margin in a patient with melanoma that developed acquired genetic resistance to ICB through a loss-of-function mutation in *JAK2*. Scale bar, 100 μm.

quartiles (Fig. 2B). This pattern was recapitulated in response to IFN-α and IFN-β (figs. S3 and S4), suggesting that MHC I expression exhibits greater IFN sensitivity in cell lines with low baseline MHC I expression.

We observed a similar IFN dependence of MHC I expression in two previously reported patients with melanoma treated with anti–PD-1 ICB who developed acquired resistance due to a loss-of-function mutation in either *JAK1* or *JAK2 (3)*. At baseline in the tumor from the patient who ultimately developed a *JAK1* loss-of-function

mutation, CD8$^+$ T cell infiltration was observed at the invasive margin (as defined by S100 expression on human melanoma; Fig. 2C, top). The S100$^+$ melanoma cells at the invasive margin adjacent to CD8$^+$ T cells expressed MHC I and PD-L1, in contrast to melanoma cells at a distance from the invasive margin. In contrast, at relapse in the *JAK1*-mutant tumor, the S100$^+$ melanoma cells in the *JAK1*-mutant tumor did not express MHC I and PD-L1; here, the MHC I and PD-L1 expression was limited to the margin surrounding the S100$^+$ melanoma cells (Fig. 2C, bottom). In a second patient whose relapsed tumor harbored a *JAK2* loss-of-function mutation, a similar absence of MHC I expression was observed on S100$^+$ melanoma cells, adjacent to an area of MHC I $^+$ stroma (Fig. 2D; baseline tumor not available). Together, these clinical data support IFN dependence of MHC I expression in patients with melanoma.

Nlrc5 overexpression bypasses IFN signaling to restore MHC I expression and sensitivity to tumor-specific T cells

We recapitulated the observed IFN dependency of MHC I expression in B16 murine melanoma. Consistent with their aberrant signaling, B16-*Ifnar1*^{KO}, B16-*Jak2*^{KO}, and B16-*Jak1*^{KO} tumors did not up-regulate surface MHC I in response to type I, type II, and both type I and II IFNs, respectively (Fig. 3A). To test the role of IFN dependence in vivo, we used B16 tumor cells overexpressing red fluorescent protein (RFP) and examined the expression of MHC I on CD45$^-$RFP$^+$ cells from tumor digests (fig. S5). RFP-labeled B16-WT, B16-*Ifnar1*^{KO}, and B16-*Jak2*^{KO} tumor cells all expressed MHC I in vivo compared to the MHC I–deficient negative control (B16-*B2m*^{KO}; Fig. 3B). However, B16-*Jak1*^{KO} tumor cells did not express MHC I in vivo, indicating that either type I or II IFN signaling is necessary to induce MHC I expression on B16 tumor cells in vivo. This

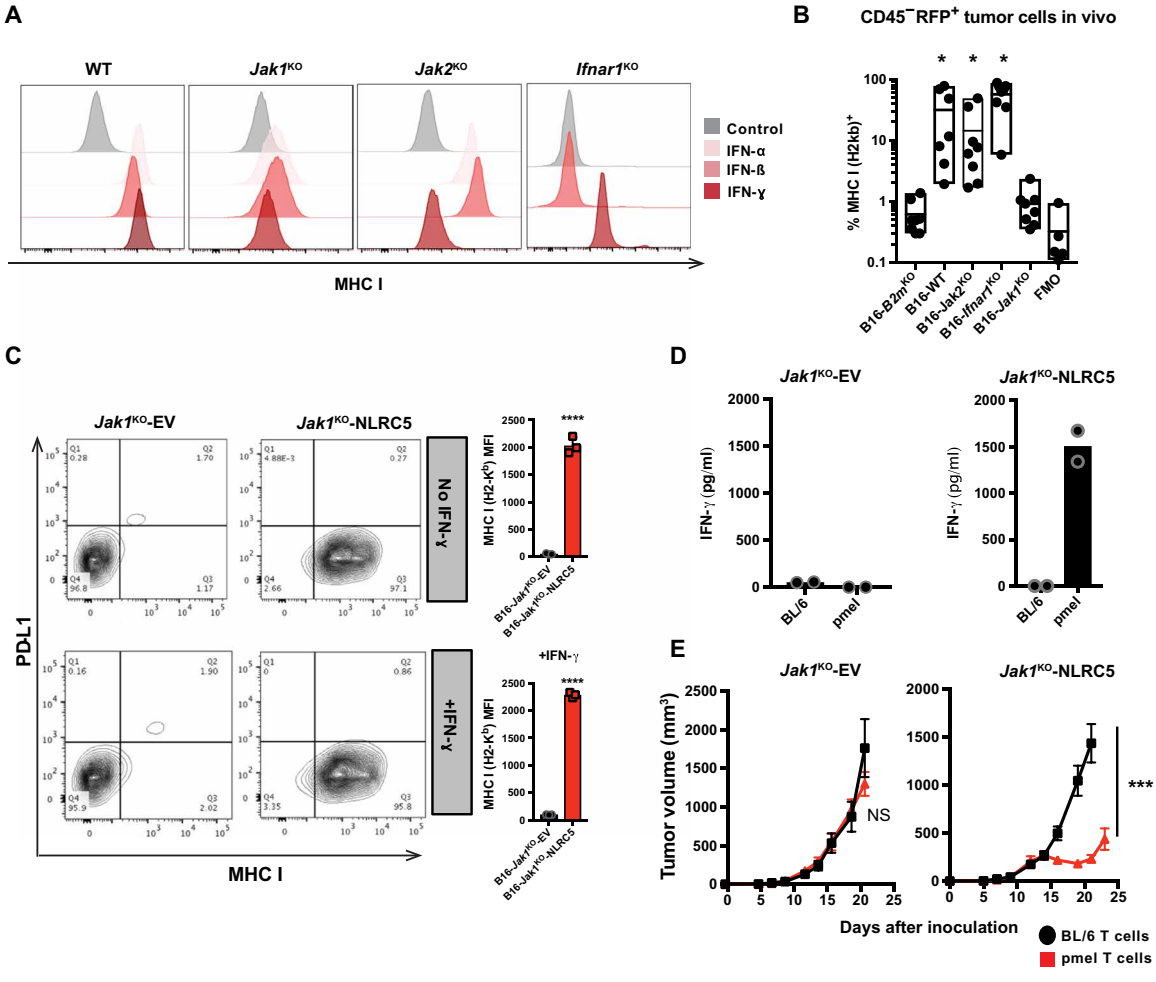

Fig. 3. NLRC5 bypasses IFN dependency of B16 MHC I expression and restores sensitivity to adoptive T cell therapy. (**A**) MHC I surface expression by flow cytometry in response to IFN-α, IFN-β, or IFN-γ in CRISPR-modified B16-F10 cell lines. (**B**) Percentage of MHC I$^+$ cells among CD45$^-$RFP$^+$ tumor cells in vivo. Mice ($n = 5$ to 8 per group) were inoculated subcutaneously with RFP$^+$ tumor cell lines. Established tumors were harvested, and single-cell suspensions were stained for CD45 and MHC I. Box plots depict minimum, maximum, and mean. (**C**) Surface expression of PD-L1 and MHC I on B16-*Jak1*^{KO} tumor cells lentivirally transduced with *Nlrc5* or empty vector control. Representative samples treated with and without IFN-γ and summary bar plots of MHC I MFI (mean ± SD, $n = 3$ per group) are shown. ****$P < 0.0001$. (**D**) IFN-γ production (mean ± SD) by BL/6 or pmel T cells after 24-hour coculture with indicated tumor cells (which were not pretreated with IFN-γ; $n = 3$ per group). (**E**) In vivo tumor growth (mean ± SEM) of B16-*Jak1*^{KO}-EV and B16-*Jak1*^{KO}-NLRC5 tumors after treatment with ACT. After lymphodepleting total body irradiation (5 Gy), tumor-bearing mice ($n = 5$ per group) were treated with ACT consisting of one dose of 5.0×10^6 pmel (or control BL/6 T cells) along with IL-2 (50,000 IU/day i.p. × 3 days). *$P < 0.05$, ***$P < 0.001$ (unpaired *t* test).

contrasts with the patient presented in Fig. 2B, where defect in type II IFN signaling alone was associated with an absence of MHC I expression.

To restore MHC I expression in IFN-deficient tumor cells, B16-*Jak1*^{KO} tumor cells were lentivirally transduced with *Nlrc5*, a transcriptional regulator of MHC I antigen-processing machinery that has been shown to induce constitutive MHC I expression in WT B16 tumor cells (*11*, *12*). Compared to those transduced with empty vector control, B16-*Jak1*^{KO}-*Nlrc5* tumor cells expressed MHC I constitutively in the presence or absence of IFN-γ (Fig. 3C). Forced expression of NLRC5 in the B16-*Jak1*^{KO} tumor cells rendered them sensitive to antigen-specific recognition by pmel T cells, as measured by IFN-γ production in vitro (Fig. 3D). Likewise, forced expression of NLRC5 restored the sensitivity of B16-*Jak1*^{KO} tumors to adoptively transferred pmel T cells and IL-2 in vivo (Fig. 3E). However, overexpression of NLRC5 in WT B16 tumors did not augment the in vivo antitumor efficacy of adoptively transferred pmel T cells and IL-2 (fig. S6). These studies demonstrate that restoring surface expression of MHC I is critical for T cell recognition in the setting of loss-of-function mutations in genes affecting IFN signaling. Still, we do not exclude other potential MHC I–independent functions for NLRC5 in the B16-Jak1^{KO} tumors.

BO-112 restores efficacy of tumor-specific T cells against tumors lacking type I and II IFN sensitivity

We reasoned that pharmacologic activation of pattern recognition receptor (PRR) pathways may activate downstream signaling pathways redundant with IFN signaling and, in so doing, restore the efficacy of tumor-specific T cells against tumors with deficient IFN signaling and insufficient MHC I expression. This would offer a pharmacological approach to up-regulate MHC I expression in immunotherapy-resistant tumors with low baseline MHC I expression. To test this hypothesis, we used BO-112, a nanoplexed formulation of poly I:C administered intratumorally. In a phase 1 study, BO-112 was found to be safe as monotherapy or in combination with anti-PD1 ICB in patients with solid tumors (*17*).

Intratumoral injection with BO-112, but not vehicle control, restored antitumor efficacy of adoptively transferred pmel T cells and IL-2 against B16-*Jak1*^{KO} tumors (Fig. 4A), similar to the effect of NLRC5 overexpression (compare with Fig. 3E). BO-112 also significantly ($P < 0.05$) augmented the antitumor efficacy of adoptively transferred pmel T cells against WT B16 tumors, although BO-112 was ineffective when used in combination with mock T cells and IL-2 (fig. S7). To evaluate the contribution of adoptively transferred and endogenous immune cells to the antitumor response, we performed parallel bulk RNA sequencing (RNA-seq) and single-cell mass cytometry of tumor specimens 5 days after ACT. By RNA-seq, the samples clustered by treatment group (control T cells and vehicle, control T cells and BO-112, pmel T cells and vehicle, and pmel T cells and BO-112) on principal component analysis (PC1 and PC3; Fig. 4B). Compared to B16-*Jak1*^{KO} tumors treated with control T cells and intratumoral vehicle injection, 700 transcripts were specifically up-regulated in tumors treated with pmel T cells and intratumoral BO-112 (hereafter referred to as the pmel–BO-112 gene set; Fig. 4C). Although we did not observe an increase in CD8 pmel T cell infiltration in the samples treated with pmel T cells and BO-112 compared to samples treated with pmel T cells and vehicle using single-cell mass cytometry (fig. S8), the pmel–BO-112 gene set was strongly correlated with infiltration of adoptively transferred CD8 pmel T cells, but not endogenous T cells (Fig. 4D). Endogenous myeloid populations, in particular polymorphonuclear myeloid-derived suppressor cells (PMN-MDSCs) and tumor-associated macrophages, were also associated with expression of the pmel–BO-112 gene set. We cannot exclude that these other cells contribute to a coordinated antitumor immune response in the group treated with pmel T cells and BO-112.

To further evaluate whether the impact of BO-112 on the antitumor efficacy in the IFN-deficient B16-*Jak1*^{KO} tumor model was dependent on recognition of tumor cells by pmel T cells via MHC I, we generated a B16-*B2m*^{KO} tumor that lacks surface MHC I due to a defect independent of IFN signaling. Like B16-*Jak1*^{KO} tumors, B16-*B2m*^{KO} tumors were also resistant to pmel T cells even after pretreatment with IFN-γ (fig. S9). However, unlike its effect on B16-*Jak1*^{KO} tumors, BO-112 did not restore the antitumor effect of adoptively transferred pmel T cells against B16-*B2m*^{KO} tumors (Fig. 4E).

BO-112 induces MHC I expression in an IFN- and Nlrc5-independent manner in murine and human melanoma

Upon exposure in vitro, BO-112 augmented the expression of surface MHC I and PD-L1 on WT B16 cells, similar to the effects of type I and II IFNs (Fig. 5, A and B, top). However, only BO-112, but not type I or type II IFNs, augmented the expression of the B16-*Jak1*^{KO} cell line (Fig. 5, A and B, bottom). Expression of MHC I antigen-processing machinery genes *B2m* and *Tap1* was augmented within 6 hours of exposure to BO-112 (Fig. 5C). Furthermore, tumor-specific IFN-γ production by pmel T cells occurred after pretreatment of WT B16 tumor cells with either BO-112 or IFN-γ. In contrast, pmel T cells only recognized B16-*Jak1*^{KO} tumor cells pretreated with BO-112, but not IFN-γ (Fig. 5D). We also evaluated the induction of MHC I by BO-112 in two human melanoma cell lines CRISPR-modified with defects in IFN signaling, M202-*JAK1*^{KO} and M407-*JAK1*^{KO}, as well as three human melanoma cell lines with low basal MHC I expression that was not inducible by IFN-γ (M311, M368, and M412B; Fig. 2A). BO-112 augmented surface MHC I expression in all cell lines except M311 (Fig. 5E).

Given the importance of *Nlrc5* in coordinating the expression of MHC I antigen-processing machinery and its position downstream of IFN signaling, we considered that the effect of BO-112 on MHC I expression may occur through induction of *Nlrc5* expression. BO-112 augmented the expression of *Nlrc5* in both WT B16 and B16-*Jak1*^{KO} tumor cells (fig. S10). To test the functional role of *Nlrc5* in MHC I expression induced by BO-112, we generated two different B16-*Nlrc5* ^{KO} tumor cell clones and two different B16-*Jak1*^{KO}-*Nlrc5* ^{KO} tumor cell clones by CRISPR. As anticipated, MHC I induction by IFN-γ was greatly diminished in B16-*Nlrc5* ^{KO} tumor cells compared to WT B16 (fig. S10). However, MHC I induction by BO-112 was retained in both B16-*Nlrc5* ^{KO} and B16-*Jak1*^{KO}-*Nlrc5* ^{KO} tumor cells (Fig. 5F and fig. S10). Thus, MHC I induction by BO-112 occurs in both an IFN- and *Nlrc5*-independent manner.

The BO-112 nanoplexed formulation of poly I:C was designed to engage dsRNA sensors. We compared the MHC I augmenting effects of BO-112 with the effects of a standard formulation of poly I:C, as well as two other PRR agonists [lipopolysaccharide (LPS), a toll-like receptor 4 (TLR4) agonist, and CpG oligonucleotides, which activate TLR9] to determine whether the effect on antigen presentation was specific to BO-112 or broadly applicable to PRR agonists. In a mouse macrophage cell line (RAW264.7) known to respond to PRR agonists (*18*), LPS, CpG, and poly I:C all resulted in an increase in MHC I expression, as did BO-112. However, aside from BO-112, none of the PRR agonists augmented MHC I expression

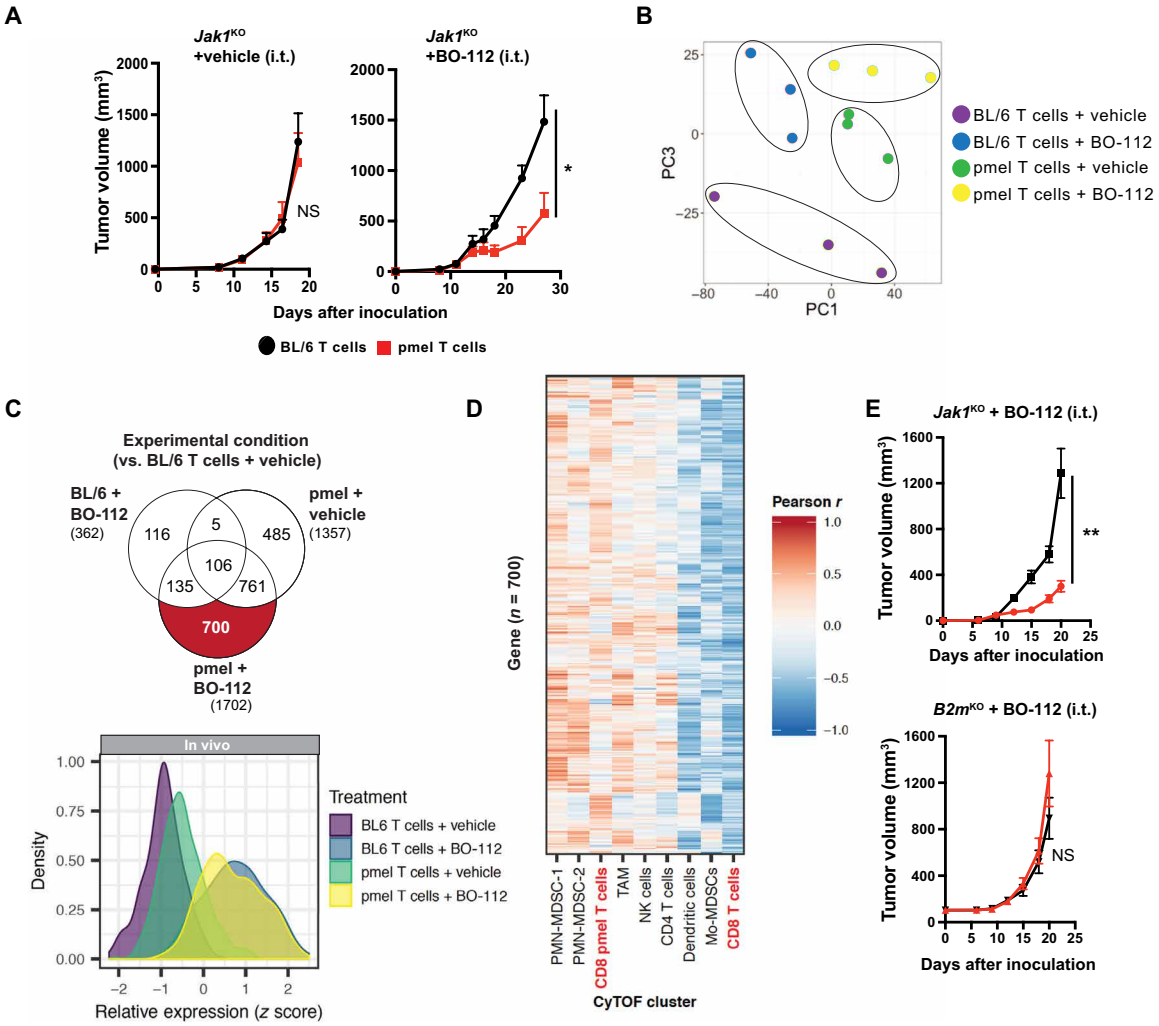

Fig. 4. BO-112 restores efficacy of tumor-specific T cells against tumor cells lacking both type I and II IFN signaling. (**A**) In vivo growth (mean ± SEM) of B16-*Jak1*^{KO} tumor cells after treatment with ACT. After lymphodepleting total body irradiation (5 Gy), tumor-bearing mice ($n = 4$ to 5 mice per group) were treated with ACT consisting of one dose of 5.0×10^6 pmel (or control BL/6 T cells) along with IL-2 (50,000 IU/day i.p. × 3 days). Left: Both groups were treated with intratumoral (i.t.) injection of vehicle control. Right: Both groups were treated with intratumoral injection of BO-112. Intratumoral injections were administered twice a week starting on the day after ACT. *$P < 0.05$ (unpaired *t* test). (**B**) Tumors were harvested 5 days after ACT (and after two doses of intratumoral vehicle or BO-112) for RNA-seq analysis ($n = 3$ per group). Principal component analysis demonstrates clustering of treatment groups by PC1 and PC3 (treatment groups encircled manually). (**C**) Top: Venn diagram illustrating the number of genes differentially expressed compared to the control group (BL/6 T cells and vehicle intratumoral agent), highlighting the 700 genes differentially expressed in the group treated with pmel ACT and intratumoral BO-112. The relative expression of this set of 700 genes is shown in the bottom panel colored by treatment group. (**D**) Heatmap of correlations between the 700 differentially expressed genes from the pmel–BO-112 gene set with CD45$^+$ populations identified by mass cytometry. Red font highlights comparison of adoptively transferred T cells (CD8 pmel T cells) and endogenous T cells (CD8 T cells). (**E**) In vivo growth (mean ± SEM) of B16-*Jak1*^{KO} tumors (top, $n = 5$ to 7 mice per group) or B16-*B2m*^{KO} tumors (bottom, $n = 7$ mice per group) after treatment with ACT and intratumoral BO-112. **$P < 0.01$ (unpaired *t* test).

of the WT B16 or B16-*Jak1*^{KO} cell lines (Fig. 5G). The surface MHC I expression of the IFN-insensitive M202-*JAK1*^{KO} human melanoma cell line increased in response to both poly I:C and BO-112, but neither LPS nor CpG, suggesting an effect specific to dsRNA sensing (Fig. 5H).

BO-112 bypasses IFN signaling to induce MHC I expression through activation of NF-κB signaling

RNA-seq analysis of the B16-*Jak1*^{KO} tumor cell line 6 hours after treatment with vehicle or BO-112 revealed a set of 190 genes differentially expressed in response to BO-112 [$P < 0.01$, false discovery rate (FDR) < 0.05, and $\log_2$(fold change) > 1.5; Fig. 6A, left]. Gene set enrichment analysis was used to identify differentially expressed gene sets ($P < 0.01$, $q < 0.05$, normalized enrichment score > 1.5) that contained at least 30 genes that were also differentially expressed, identifying eight significantly different gene sets that were up-regulated in BO-112–treated B16-*Jak1*^{KO} cells, compared to vehicle-treated B16-*Jak1*^{KO} (Fig. 6A, right). Despite the absence of IFN signaling in B16-*Jak1*^{KO} tumor cells, BO-112 induces an "IFN-like" gene signature, highlighted by genes in the Hallmark IFN-γ Response Pathway, the Hallmark IFN-α Response Pathway, and the Reactome IFN Signaling gene sets. To determine whether the tumor-intrinsic effects of BO-112 in vitro were also observed in vivo, we examined the genes that were specifically up-regulated in B16-*Jak1*^{KO} tumors treated with BO-112 and either pmel or control T cells (135 genes; Fig. 6B). Of these 135 genes, 55 were significantly

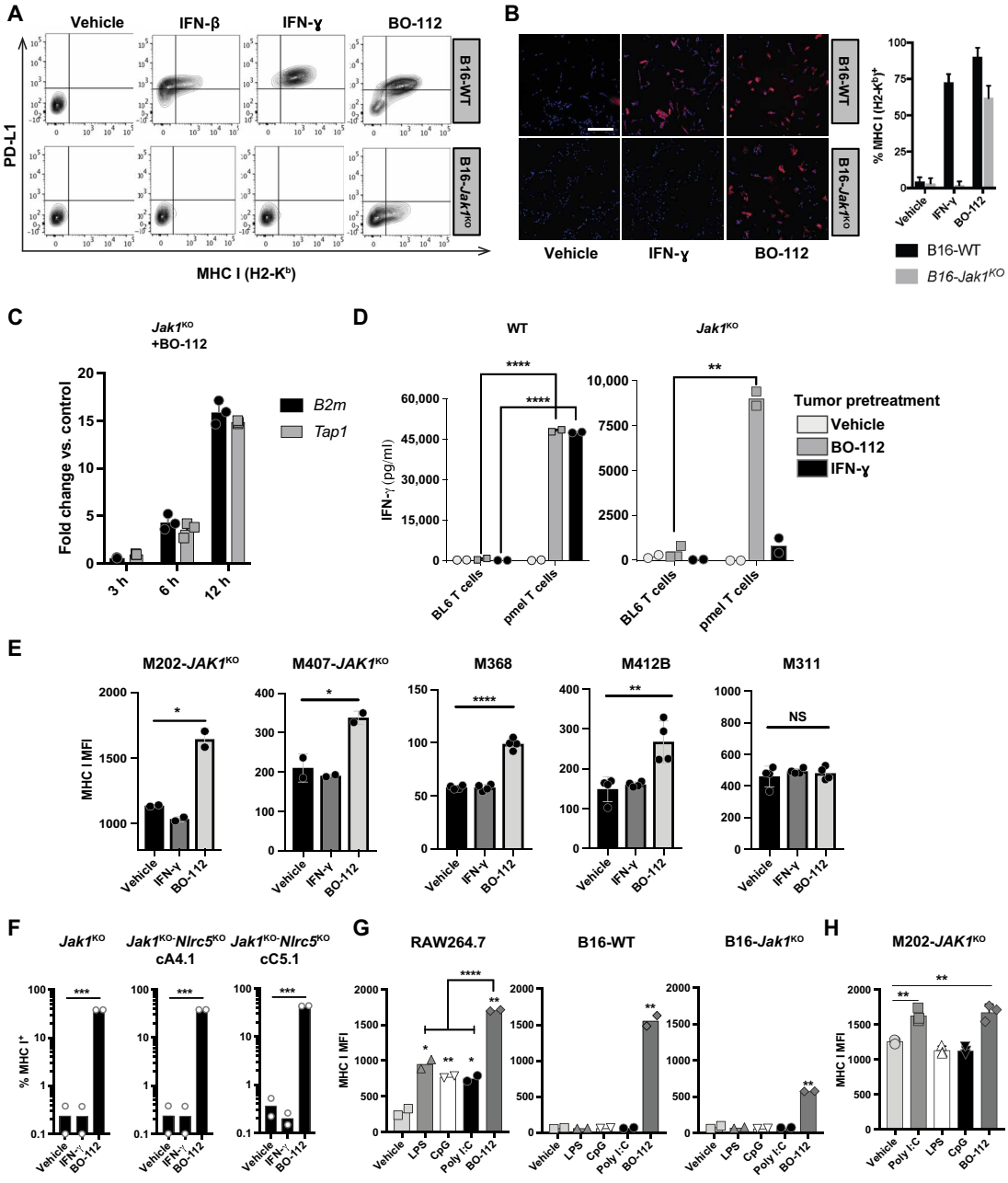

Fig. 5. BO-112 induces MHC I expression in an IFN- and *Nlrc5*-independent manner. (**A**) Surface expression of PD-L1 and MHC I (H-2K^b) on B16-WT and B16-*Jak1*^{KO} cell lines after 18-hour exposure to IFN-β, IFN-γ, or BO-112. (**B**) Immunofluorescence images of B16-WT and B16-*Jak1*^{KO} cell lines treated as in (A) and stained with PE-conjugated anti-mouse MHC I (H-2K^b) and 4′,6-diamidino-2-phenylindole (DAPI) nuclear staining, with quantification in the right panel (mean ± SD; $n = 48$ samples per treatment group). Scale bar, 20 μm. (**C**) Expression of genes (mean ± SD) involved in MHC I antigen-processing machinery (*B2m* and *Tap1*) by quantitative RT-PCR in BO-112–treated B16-*Jak1*^{KO} tumor cells after 3, 6, and 12 hours, relative to vehicle-treated control ($n = 3$ per group). (**D**) IFN-γ production (mean ± SD) by T cells (activated BL6 T cells or pmel T cells) in coculture with B16-WT and B16-*Jak1*^{KO} tumor cells pretreated with vehicle, BO-112, or IFN-γ ($n = 3$ per group). (**E**) Effect of IFN-γ and BO-112 on surface MHC I expression (mean ± SD) of five human melanoma cell lines ($n = 2$ to 4 per group), including two with known defects in IFN signaling (M202-*JAK1*^{KO} and M407-*JAK1*^{KO}) and three cell lines with low basal MHC I expression (see Fig. 2A). (**F**) B16-*Jak1*^{KO} tumor cells were modified using CRISPR with guides targeting *Nlrc5* to generate two clonal B16-*Jak1*^{KO}-*Nlrc5*^{KO} cell lines (cA4.1 and cC5.1). The percentage of MHC I$^+$ in each tumor cell line (mean ± SD) after treatment with IFN-γ or BO-112 for 18 hours ($n = 3$ per group) is shown. (**G** and **H**) MHC I mean fluorescence intensity (mean ± SD) in response to a panel of PRR agonists [LPS (100 ng/ml), CpG (10 μg/ml), poly I:C (100 μg/ml), and BO-112 (0.5 μg/ml)] in mouse (G) and human (H) cell lines (RAW246.7 macrophages, B16-WT and B16-*Jak1*^{KO} mouse melanoma, and M202-*JAK1*^{KO} human melanoma; $n = 2$ to 3 per group). *$P < 0.05$; **$P < 0.01$; ***$P < 0.001$; ****$P < 0.0001$ (unpaired *t* test).

increased both in vitro and in vivo in groups treated with BO-112 [$P < 0.01$, FDR < 0.05, and $\log_2$(fold change) > 1.5; Fig. 6B]. Notably, 23 of these 55 genes were involved in either type I IFN signaling or TNF-α signaling via NF-κB (Fig. 6C).

We postulated that NF-κB could be the transcriptional effector of the signaling induced by BO-112 that was responsible for IFN- and *Nlrc5*-independent MHC I expression. Treatment with BO-112 augmented cytoplasmic phosphorylation and nuclear translocation of NF-κB (p65) (fig. S11). We treated our B16-*Jak1*^{KO} cell line with BO-112 in conjunction with a selective NF-κB inhibitor, BMS-345541. BMS-345541 abrogated the induction of MHC I by BO-112 in a dose-dependent manner (Fig. 7A). A transient knockdown of *Rela* via two different small interfering RNAs (siRNAs) achieved a similar effect, inhibiting the up-regulation of surface MHC I by BO-112 in B16-*Jak1*^{KO} tumors, as well as in human melanoma M407-JAK1^{KO} (Fig. 7B).

We screened the effects of siRNA targeting four putative dsRNA sensors on induction of MHC I by BO-112. Knockdown of *Pkr* and *Tlr3*, both of which are known to directly signal through NF-κB (*19*–*21*), but not *Ifih1* or *Ddx58*, abrogated MHC I induction by

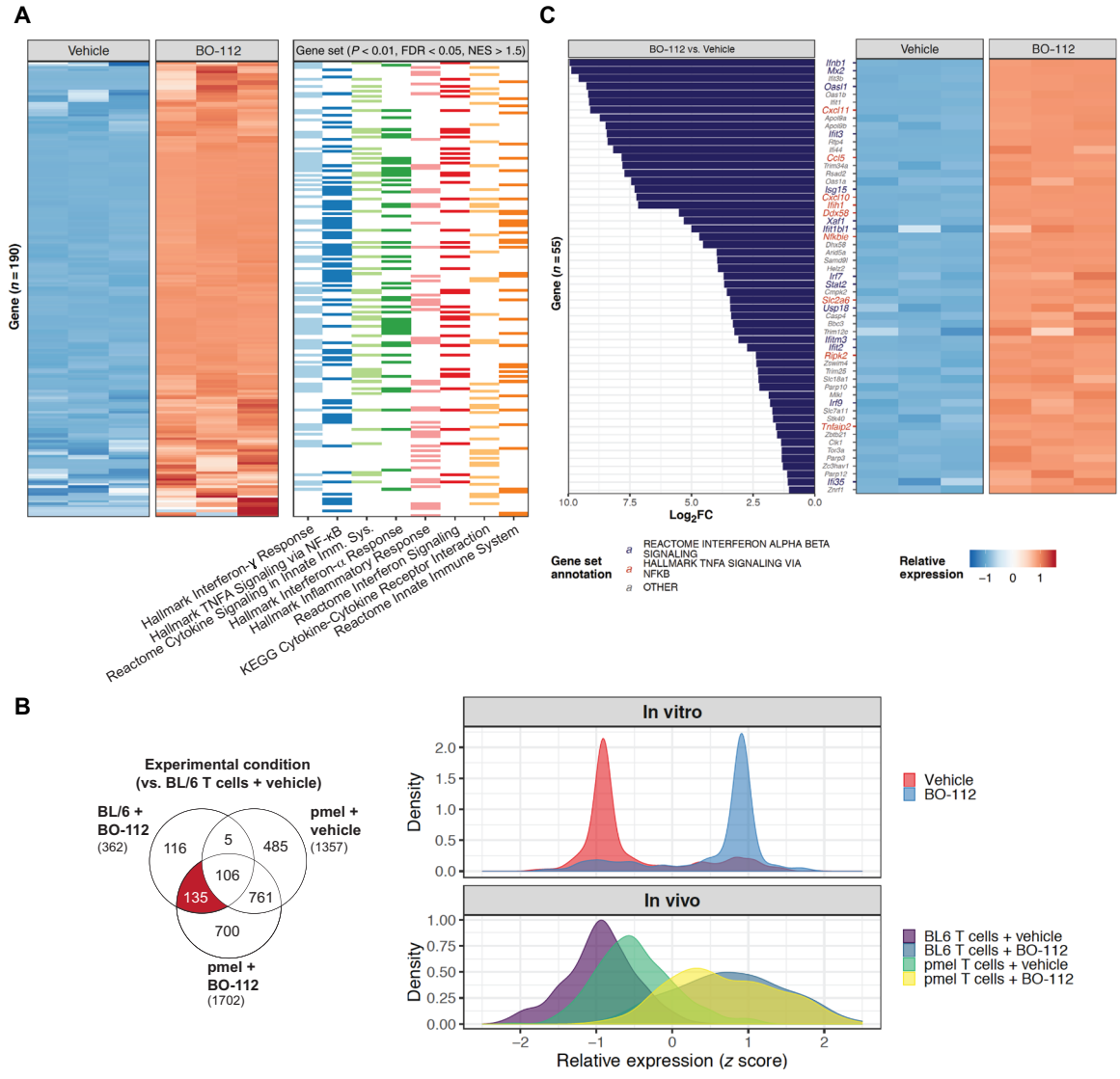

Fig. 6. BO-112 induces IFN and NF-κB gene expression programs in B16-*Jak1*^{KO} tumor cells despite the absence of IFN signaling. (**A**) B16-*Jak1*^{KO} tumor cell lines were treated with vehicle or BO-112 for 6 hours, and gene expression was quantified by RNA-seq ($n = 3$ biological replicates). The left panel shows the top 190 differentially expressed genes [$P < 0.01$, FDR < 0.05, and $\log_2$(fold change) > 1.5], which were also associated with significantly enriched gene sets [$P < 0.01$, FDR < 0.05, and normalized enrichment score (NES) > 1.5]. The eight enriched gene sets with at least 30 differentially expressed genes are shown in the right panel. (**B**) Comparison of the 136 genes enriched in tumors treated with BO-112 from our in vivo experiment (left; see also Fig. 4) with genes enriched in B16-*Jak1*^{KO} tumor cell line treated with BO-112. Relative expression of these 136 genes in the cell lines (right, top) mirrors the expression of these same genes in the groups treated with BO-112 in vivo (right, bottom). (**C**) Left: Illustration of the in vitro $\log_2$(fold change) of 55 genes specific to BO-112 treatment both in vitro and in vivo. Enrichment of type I IFN signaling (blue font) and TNF-α signaling via NF-κB (red font) gene sets is highlighted and shown in larger font. Right: Relative expression of each gene in vitro.

BO-112 (Fig. 7C and fig. S12). Of these, only siRNA against PKR (protein kinase R) completely abrogated the effect of BO-112 on MHC I induction. Consistent with the hypothesis that BO-112 activates NF-κB signaling via PKR, siRNA targeting PKR reduced the abundance of nuclear NF-κB (p65) in response to BO-112 (Fig. 7D).

DISCUSSION

Although ICB is effective in a subset of patients with melanoma and other malignancies, most patients still do not benefit. Tumor defects in IFN signaling are an important mechanism of both primary and acquired resistance to ICB (*3*, *4*, *6*, *8*, *22*). This role of IFN signaling is consistent with preclinical studies that demonstrated the importance of tumor IFN sensitivity in mounting an effective antitumor immune response (*1*, *2*). Accordingly, we observed resistance to the combination of dual ICB and focal radiation in B16 murine melanoma with defects in *Jak1* or *Jak2* observed in patients with acquired resistance to ICB.

We queried whether T cell–based ACT could be an effective approach to overcome resistance in tumors with defective IFN signaling, especially given the increased utilization of ACT with tumor-infiltrating lymphocytes and TCR- or CAR-engineered T cells for patients with cancer. Notably, the efficacy of ACT with tumor-specific pmel T cells was unaffected by defects in *Jak2* or *Ifnar1* in

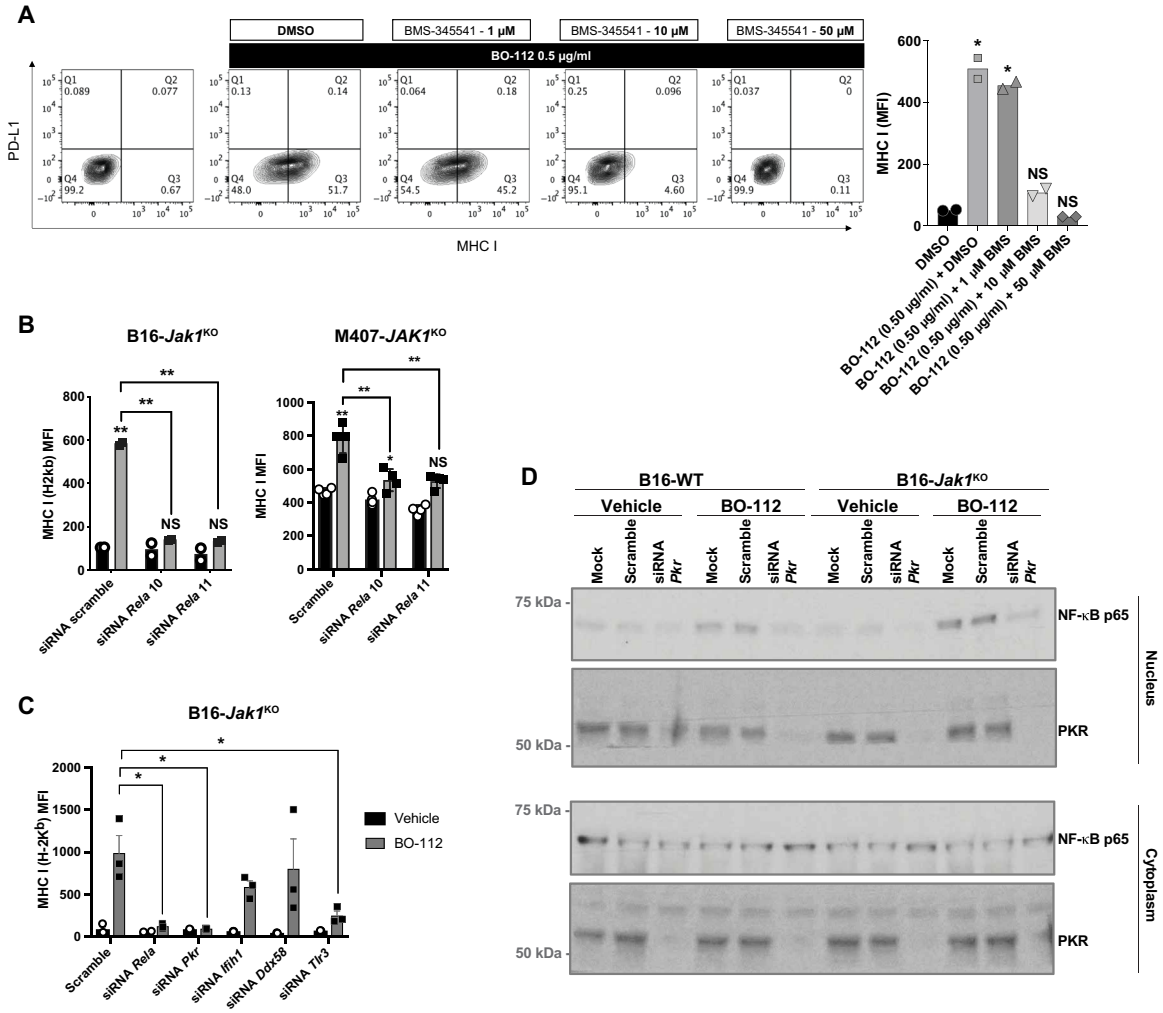

Fig. 7. BO-112 bypasses IFN signaling and induces MHC I expression through direct dsRNA sensor-mediated activation of NF-κB signaling. (**A**) Surface expression of MHC I and PD-L1 in B16-*Jak1*^{KO} tumor cells (representative example) treated with increasing doses of BMS-345541, a selective NF-κB inhibitor. Right: Quantification (mean with individual data points; $n = 2$ per group). *$P < 0.05$ (unpaired t test). DMSO, dimethyl sulfoxide. (**B**) Effect of siRNA targeting *Rela* on expression of MHC I in mouse B16-*Jak1*^{KO} (mean, $n = 2$ per group) and human M407-*JAK1*^{KO} (mean ± SD; $n = 4$ per group) tumor cells in response to BO-112. *$P < 0.05$; **$P < 0.01$ (unpaired t test). (**C**) Impact of siRNAs against dsRNA sensors (*Pkr*, *Ifih1*, *Ddx588*, and *Tlr3*), as well as *Rela*, on the induction of MHC I by BO-112 (mean ± SD; $n = 3$ per group). *$P < 0.05$ (unpaired t test). (**D**) Effect of siRNA targeting *Pkr* on expression of nuclear and cytoplasmic NF-κB (p65) in mouse B16-WT and B16-*Jak1*^{KO} tumor cells in response to BO-112.

B16 tumors. However, ACT with pmel T cells was ineffective against B16-*Jak1*^{KO} tumors lacking both type I and II IFN signaling both in vitro and in vivo.

Our findings indicate that either type I or II IFN signaling is necessary to coordinate MHC I antigen presentation by B16 tumor cells in vivo and thereby confer sensitivity to pmel ACT. The role of IFN signaling in the coordinated expression of MHC I antigen-processing machinery (including peptide processing and transportation) is well described (*16*, *23*), and melanoma tumors with defective MHC I expression and IFN signaling have been reported (*4*). MHC I expression on B16 is absent in vitro at baseline and readily inducible by IFN (*24*, *25*). This phenotype of low basal and IFN-inducible MHC I expression is not unique to B16 murine melanoma. Although human melanoma cell lines have variable expression of MHC I, we found that a subset can also exhibit poor basal expression of MHC I that can be induced by type I or II IFNs. In addition, in relapsed tumors from patients after anti–PD-1 ICB with absent IFN signaling, the putative IFN-dependent gradient of MHC I expression at the tumor margin was no longer observed. Others have also reported that melanoma lesions progressing in the context of immune-based therapies have weak MHC I expression (*26*, *27*).

We used NLRC5 as a tool to restore constitutive MHC I expression in the IFN signaling–deficient B16-*Jak1*^{KO} model and, in doing so, restored the antitumor efficacy of pmel ACT. Thus, when MHC I is constitutively expressed, the absence of tumor IFN signaling does not negate the efficacy of tumor-specific CD8$^+$ T cells. This is consistent with the capacity of effector T cells to directly kill tumor cells in a perforin- and granzyme-dependent manner, independent of IFN signaling (*10*).

Our findings also highlight the different mechanisms that drive resistance to ICB and ACT. IFN signaling has diverse downstream effects, including direct antiproliferative effects (*28*, *29*), the induction of immune checkpoints such as PD-L1 (*30*, *31*), the expression of T cell chemoattractants CXCL9 and CXCL10 (*32*–*34*), and the

coordinated expression of antigen presentation machinery. In the context of ICB, the complex interplay of each of these factors may drive response or resistance (*9*). In some model systems, defects in IFN signaling have even resulted in improved efficacy of ICB (*15*, *35*). In other scenarios, antigen presentation can be defective despite intact IFN signaling (*36*). In the context of T cell–based ACT, our results suggest that the role of tumor IFN signaling is primarily tied to its effect on antigen presentation. From this, we infer also that CAR T cells, which target tumors independent of MHC expression, would also be effective against IFN-deficient tumors.

In the absence of IFN signaling, alternative means to induce MHC I expression are needed. BO-112 is a nanoplexed formulation of poly I:C that activates dsRNA sensors such as TLR3, MDA5, RIG-I, and PKR. When administered intratumorally in phase 1 studies in combination with anti–PD-1 ICB, BO-112 can induce clinical responses in patients refractory to anti–PD-1 therapy alone (*13*). We found that BO-112 can induce MHC I expression in IFN signaling–deficient melanoma and thus restore the antitumor activity of pmel ACT. However, BO-112 restored MHC I expression through an NF-κB–mediated mechanism and independent of NLRC5. NF-κB is a known regulator of MHC I expression, especially at the human leukocyte antigen A (HLA-A) locus (*37*–*39*), and is directly activated by dsRNA sensors TLR3 (*21*) and PKR (*19*, *20*). Among canonical dsRNA sensors, *Pkr* and *Tlr3* mediated the effect of BO-112 on MHC I in B16 melanoma. These findings are consistent with the capacity of the West Nile virus, a single-stranded RNA virus, to induce MHC I in mouse embryonic fibroblasts in an NF-κB–dependent and IFN-independent manner (*40*).

There is also emerging literature on the role for tumor cell–intrinsic dsRNA sensing in response and resistance to immunotherapy. Tumor cell–intrinsic dsRNA sensing via RIG-I was shown to be critical for response to ICB, though in IFN-replete models (*41*). As another example, loss of ADAR1 in B16 tumor cells, for example, amplified dsRNA sensing and sensitized B16 tumors to anti–PD-1 and GVAX immunotherapy (*42*). Our findings illustrate a mechanism by which dsRNA sensing can restore sensitivity to T cell–based ACT.

Our study has limitations. First, our modeling does not account for the resistance of patients harboring tumors with sufficient basal expression of MHC I despite tumor-intrinsic IFN defects. Although we demonstrated that BO-112 can also augment the efficacy of ACT against tumors with low MHC I expression that retain IFN sensitivity, the contribution of IFN-independent MHC I induction is less likely a major factor in this context. Second, the direct effects of BO-112 on tumor cells are limited to injected lesions. Systemic delivery of a tumor-specific dsRNA agonist may maximize the therapeutic potential of this approach. Third, although we used Janus kinase 1 (JAK1) and JAK2 knockout models to model IFN insensitivity, these kinases are also involved in pathways other than IFN signaling. To address this, we conducted studies using IFN-α, IFN-β, and/or IFN-γ as stimuli to highlight the specific role of IFN signaling in each knockout model.

In conclusion, we propose that T cell–based ACT can still be an effective immunotherapy approach in tumors with JAK2 loss that are resistant to ICB, so long as there is sufficient antigen presentation. In the absence of IFN-inducible antigen presentation, such as in tumors with JAK1 loss, activation of dsRNA PRR sensors by BO-112 provides an IFN-independent approach to restore MHC I expression via NF-κB and sensitize tumors to the direct antitumor effect of $CD8^+$ T cell–based ACT.

MATERIALS AND METHODS

Study design

We examined the effect of tumor-intrinsic defects in IFN signaling on the antitumor efficacy of tumor-specific T cells. We used syngeneic mouse melanoma cell lines (B16-F10) with CRISPR-generated deficits in either type I, type II, or both type I and II IFN signaling. Treatments included tumor-specific pmel T cells (or tumor-nonspecific C57BL/6 T cells as a control) and BO-112, a nanoplexed formulation of poly I:C delivered intratumorally (or its vehicle as a control). We performed in vivo adoptive cell transfer studies and in vitro coculture experiments and measured tumor growth, activation of T cells, and gene and protein expression. Mice were randomized to treatment groups after tumors were established to ensure consistent tumor sizes. Numbers of mice per group and statistical analysis are described in more detail in the figure legends and statistical methods. Infrequently (less than 10% of all cases), an outlier tumor was identified by size before initiation of treatment (as determined by Grubbs' test) and excluded from analysis. Tumors were measured by an individual blinded to treatment groups. In vivo experiments are representative of at least two replicates. For in vitro experiments, biological duplicates or triplicates were tested, and experiments are representative of at least two replicates.

Cell lines

The B16-F10 mouse melanoma cell line and RAW264.7 were purchased from the American Type Culture Collection (ATCC). B16-F10, RAW264.7, and patient-derived human melanoma cell lines were cultured with complete medium (RPMI 1640 with L-glutamine, Thermo Fisher Scientific) containing 10% fetal bovine serum (FBS) (Omega Scientific), penicillin (100 U/ml; Omega Scientific), streptomycin (100 μg/ml; Omega Scientific), and amphotericin B (0.25 μg/ml; Omega Scientific). Mouse T cells were cultured in complete medium supplemented with 10% FBS (HyClone Characterized Fetal Bovine Serum), antibiotics, and 50 μM 2-mercaptoethanol (Gibco). Cell lines were confirmed to be mycoplasma negative using a mycoplasma detection kit (Biotool #B3903) and periodically tested for authentication. For in vivo experiments, early-passage cell lines were used (less than 10 passages).

Animals

Pmel-1 TCR/Thy1.1 transgenic mice on a C57BL/6 background were obtained from The Jackson Laboratory. C57BL/6 mice were obtained from a defined-flora, pathogen-free colony at the Association for the Assessment and Accreditation of Laboratory Care–approved animal facility of the Department of Radiation Oncology, University of California, Los Angeles (UCLA). All mice were bred, kept, and used in this colony under a UCLA Animal Research Committee–approved protocol.

CRISPR-Cas9 knockout

For human melanoma cell lines M407 and M202, CRISPR-Cas9 mediated knockouts of *JAK1* were generated as previously described (*3*). For mouse cell lines, CRISPR-Cas9 gene targeting was accomplished by first cloning the guide sequence selected using the CRISPOR program into the pSpCas9(BB)-2A-GFP vector (Addgene) containing an ampicillin resistance gene (*43*, *44*). The sequences for each guide used are listed in table S1. DNA was isolated from Transformed One Shot Stbl3 Chemically Competent *E. coli* (Invitrogen) colonies selected by ampicillin resistance and verified using the U6

promoter primer forward 5-GCCTATTTCCCATGATTCCTTC-3. Mouse tumor cell lines were transfected using Lipofectamine 3000 reagent (Thermo Fisher Scientific) and single cell–sorted from the bulk population by green fluorescent protein (GFP) expression (Aria II, BD Biosciences). Expanding clones were screened for successful CRISPR modification using targeted polymerase chain reaction (PCR) amplification of the single guide RNA (sgRNA) target region (HotStarTaq Master Mix, Qiagen), followed by Sanger sequencing. Successful targeting of genes of interest was determined by tracking of indels by decomposition analysis (Netherlands Cancer Institute; https://tide.nki.ni). CRISPR knockouts of genes responsible for IFN signaling (*Jak1*, *Jak2*, and *Ifnar1)* were further confirmed by functional assessment of surface MHC I and PD-L1 expression in response to IFNs (Fig. 1A). CRISPR knockout of *B2m* was confirmed by surface MHC I expression after IFN treatment. As a control cell line for the CRISPR process, we used a WT B16 clone (B16-WT) in which targeting of the genes of interest was unsuccessful (B16-WTCC).

Evaluation of surface MHC I and PD-L1 expression

Cell lines were seeded in complete medium containing IFN-γ (100 ng/ml) (PeproTech, catalog no. 315-05), IFN-β (500 IU/ml) (Merck Millipore, catalog no. IF011), IFN-α (500 IU/ml) (Merck Millipore, catalog no. IF009), BO-112 (0.5 to 1.0 μg/ml; Highlight Therapeutics), BMS-345541 (Sigma-Aldrich), or phosphate-buffered saline (PBS) for 18 hours. In other experiments, cells were treated with LPS (100 ng/ml; InvivoGen, #tlrl-b5lps), CpG oligodeoxynucleotides (10 μg/ml; InvivoGen, #tlrl-1826), or poly I:C (100 μg/ml; InvivoGen, #tlrl-pic). After 18 hours, cells were harvested with 10 mM EDTA (Sigma-Aldrich) and surface-stained in PBS, 5% FBS, and 2 mM EDTA with allophycocyanin (APC) anti-mouse H-2K^b (BioLegend #116518, clone AF6-88.5) and phycoerythrin (PE) anti-mouse PD-L1 (BioLegend #155404, clone MIH7) for murine tumor cells, and with PE-Cy7 anti-human HLA-A,B,C (BioLegend #311430, clone W6/32) and APC anti-human PD-L1 (BioLegend #374514, clone MIH3) for human tumor cells. Cells were analyzed by flow cytometry using LSR II (BD Biosciences). Data were analyzed using the FlowJo software (version 10.6.1).

Generation of tumor-specific murine T cells

Splenocytes from pmel transgenic mice were cultured in complete medium (as described above) plus murine IL-2 (50 U/ml; PeproTech) and pulsed with murine gp100 peptide (1 μg/ml; Thermo Fisher Scientific). C57BL/6 mice were used as a control, and splenocytes were cultured in T cell medium and murine IL-2 (50 U/ml; PeproTech) and pulsed with anti-CD3 and anti-CD28 antibodies (1 μg/ml). Expanded T cells were then washed and cultured in murine IL-2 (50 U/ml) and used for in vivo adoptive cell transfer or in vitro coculture experiments between days 3 and 9.

Tumor cell proliferation assay

Cell lines were transduced with a nuclear localizing RFP (NucLight Red Lentivirus EF1a Reagent, Essen Biosciences) to facilitate cell counts. B16-WT and knockout cell lines (RFP$^+$) were pulsed with IFN-γ (100 ng/ml) and IFN-β (500 IU/ml) 18 hours before coculture and BO-112 (0.5 μg/ml) (Highlight Therapeutics) 6 hours before coculture. After 18 hours, RFP$^+$ murine melanoma cells were harvested using 10 mM EDTA and plated in a flat-bottom 96-well plate in triplicate for each condition at 5000 cells per well for IncuCyte Live-Cell Analysis (Essen Bioscience). Pmel-1 T cells and C57BL/6 splenocytes were added at 2:1 effector-to-target ratio. At least two phase-contrast and fluorescent images were obtained of each well every 2 hours using the IncuCyte live imaging system for at least 72 hours. Images were quantified by percentage confluence of the fluorescent signal.

Enzyme-linked immunosorbent assay

B16-WT and knockout cell lines (RFP$^-$) were pulsed with IFN-γ (100 ng/ml) and IFN-β (500 IU/ml) 18 hours before coculture and BO-112 (0.5 μg/ml) 6 hours before coculture. Target tumor cells were harvested using 10 mM EDTA and plated in a round-bottom 96-well plate in triplicate for each condition at 100,000 cells per well. Pmel-1 T cells and C57BL/6 splenocytes were added at 1:1 effector-to-target ratio. The cocultured cells were incubated at 37°C for 24 hours. Supernatant was then harvested and frozen at −20°C. Coculture supernatants were thawed and analyzed by enzyme-linked immunosorbent assay for mouse IFN-γ (Thermo Fisher Scientific) according to the manufacturer's instructions.

Gene expression assays

Total RNAs were extracted using the PureLink RNA Mini Kit (Invitrogen) or RNeasy Mini Kit (Qiagen). Gene expression was then measured using the Power SYBR Green RNA-to-CT 1-Step Kit (Thermo Fisher Scientific) according to the manufacturer's instructions. Reverse transcription PCR (RT-PCR) was performed with the ViiA 7 Real-Time PCR System (Thermo Fisher Scientific). Data were normalized to 18*S* expression.

Immunohistochemistry

Tumor samples were obtained and slides were stained as previously described (*3*). Briefly, staining was performed at the UCLA Translational Pathology Core Laboratory using Leica Bond ancillary reagents and REFINE Polymer DAB detection system. Briefly, slides were stained with S100 (Dako), CD8 (Dako), PD-L1 (clone SP142, Spring Bio), and MHC I (clone HC 10, Sapphire NA) and scanned at 40× on an Aperio ScanScope AT (Leica Biosystems).

Murine NLRC5 plasmid design

Total RNA was obtained from murine splenocytes using the PureLink RNA Mini Kit (Invitrogen) according to the manufacturer's instructions. Total RNA was then reverse-transcribed to complementary DNA (cDNA) using the Superscript IV Reverse Transcriptase Kit (Thermo Fisher Scientific) with an Oligo(dT)20 primer (Thermo Fisher Scientific). The cDNA was then amplified using the Phusion High-Fidelity PCR Kit (New England BioLabs) and primers specific for the NLRC5 coding sequence. A Gibson Assembly kit (New England BioLabs) was used to incorporate the NLRC5 PCR product into the pRRL-MSCV viral plasmid and confirmed by Sanger sequencing.

Lentiviral vector production and gene transfer

Lentivirus was achieved by cotransfection of 293T cells (ATCC). Poly-L-lysine (Sigma-Aldrich)–coated tissue culture plates were seeded with 5×10^6 293T cells and allowed to adhere. Medium was then replaced with complete medium without FBS. Cells were transfected with pRRL-MSCV-mNLRC5 (5 μg) or pRRL-MSCV-mGFP (5 μg), along with pCMV8.9 (5 μg) and pCAGGS-VSV-G (1 μg) using TransIT-293 Transfection Reagent (Mirus Bio). After 17 hours, the medium was replaced with Dulbecco's modified

Eagle's medium (DMEM) with 10% FBS containing 20 mM Hepes (Invitrogen) and 10 mM sodium butyrate (Sigma-Aldrich). After 8 hours, cells were washed and replenished with complete DMEM with 20 mM Hepes. After 24 hours, the supernatants were collected, filtered through 0.45-μm filters, and stored at −80°C. For transduction, B16-WT and B16-*Jak1*^{KO} tumor cells at 40 to 60% confluence were incubated with viral supernatant along with polybrene (8 μg/ml) (Sigma-Aldrich). After 12 to 16 hours, medium was replaced and cells were expanded and sorted (Aria II, BD Biosciences) on the basis of augmented basal expression of MHC I.

In vivo ACT studies

B16-WT or CRISPR-modified cells (5×10^5) were injected subcutaneously in the right flank of C57BL/6 mice (6 to 10 weeks of age). Female mice were used to match the sex of the pmel mice from which adoptively transferred T cells were derived. Seven days after tumor inoculation, mice were treated with lymphodepleting (500 cGy) total body irradiation. On day 9, 4.0×10^6 to 5.0×10^6 gp100-activated pmel-1 T cells (or control BL/6 T cells) were adoptively transferred (intravenously) to mice bearing palpable tumors (~50 mm^3). Mice were also treated with recombinant human IL-2 (50,000 IU per day, intraperitoneally) for three consecutive days starting on the day of adoptive transfer. Beginning the day after adoptive transfer, BO-112 was administered via intratumoral injection at 2.5 mg/kg, twice a week for a total of three doses. Tumor size (length × width) was monitored every 2 to 3 days, and volume was calculated as (length × width^2)/2.

In vivo ICB studies

B16-WT or CRISPR-modified cells (5×10^5) were injected subcutaneously in bilateral flanks of C57BL/6 mice (6 to 10 weeks of age) on day 0. When tumors reached a volume of at least 50 mm^3, mice were randomized into different treatment groups according to the experimental plan. InVivoMab anti-mouse PD-1 (reference no. BE0146) and anti-mouse CTLA-4 (reference no. BE0131) or their corresponding isotypes, anti-trinitrophenol [rat immunoglobulin G2a (IgG2a), reference no. BE0089] and polyclonal Syrian hamster IgG (reference no. BE0087) from Bio X Cell, were administered by intraperitoneal injection (200 μg per antibody per dose). Focal tumor–directed computed tomography–guided radiation was delivered using the Small Animal Radiation Therapy platform (Precision X-Ray) with mice anesthetized using isoflurane. Tumors were measured daily until the animals died or the tumor volume reached 2000 mm^3.

siRNA experiments

Cells were plated in triplicate for each siRNA condition. After 8 hours, cells were transfected with scrambled or on-target siRNAs (see table S2) using Lipofectamine RNAiMAX (Thermo Fisher Scientific, catalog no. 13778150) according to the manufacturer's guidelines. Alternatively, cells were transfected with ON-TARGETPlus siRNA Pools for PKR or Non-targeting Control (siNTC) (Dharmacon). After 48 to 72 hours of transfection, medium was replaced with fresh medium containing either BO-112 (0.5 μg/ml; Highlight Therapeutics) or vehicle (5% glucose in PBS). After 6 or 18 hours, cells were harvested with 10 mM EDTA in PBS and analyzed by flow cytometry or harvested for downstream protein analysis by Western blot.

Western blot

Nuclear and cytoplasmic protein fractions were obtained by using the NE-PER Nuclear and Cytoplasmic Extraction Kit (Pierce) according to the manufacturer's instructions. Antibodies are listed in table S2.

Mass and flow cytometry of in vivo tumor specimens

Single-cell suspensions of tumors harvested from mice were stained as previously described (*45*). Briefly, tumors were minced and dissociated using a murine tumor dissociation kit (Miltenyi Biotec, catalog no. 130-096-730) and the gentleMACS Octo Dissociator (Miltenyi Biotec, catalog no. 130-095-937). Cells were then resuspended in PBS and filtered through a 70-μm cell strainer to obtain single-cell suspensions. For mass cytometry, the single cells were first stained with Cell-ID Cisplatin (1:2500 dilution; Fluidigm, catalog no. 201064) for 5 min at 37°C. Cells were then washed with PBS and stained with the surface antibody cocktail for 30 min at room temperature. Cells were again washed and fixed with 1.6% formaldehyde for 20 min at room temperature. After fixation, cells were then washed with Maxpar Perm-S Buffer (Fluidigm, catalog no. 201066) and stained with the intracellular antibody cocktail for 30 min at room temperature. Last, cells were stained with the intercalating solution (Cell-ID Intercalator-Ir, catalog no. 201192B) at a 1:6000 dilution in Maxpar Fix and Perm Buffer (Fluidigm, catalog no. 201067) overnight at 4°C. For flow cytometry experiments, cells were first stained in PBS with viability dye (Zombie UV Fixable Viability Kit, BioLegend, catalog no. 423107) and then washed and stained with surface antibodies in PBS, 5% FBS, and 2 mM EDTA. Antibodies are listed in table S2. Data were acquired using a Fluidigm Helios mass cytometer or an LSR II (BD Biosciences) flow cytometer. For mass cytometry data, manually gated CD45$^+$ populations (FlowJo software version 10.4.2) were analyzed using cytofkit package (R version 3.5.1). Dimensionality reduction using *t*-SNE (*t*-distributed stochastic neighbor embedding) algorithm was performed on each dataset, and plots were generated by PhenoGraph clustering through cytofkitShinyAPP from cytofkit (*46*). Flow cytometry data were analyzed in FlowJo software (version 10.6.1).

RNA-seq and analysis

Murine subcutaneous tumors were harvested and stored in RNAlater overnight at 4°C before transferring to −80°C. Total RNA was extracted from tumors or cell lines using the AllPrep DNA/RNA Micro Kit (Qiagen). RNA-seq libraries were prepared using a KAPA mRNA stranded library preparation kit, according to the manufacturer's recommendations. Libraries were pooled and sequenced on the Illumina HiSeq3000 platform [50–base pair (bp) reads]. Reads were aligned to the mouse reference genome (mm9/GRCm38) using HISAT2 (v2.0.4) (*47*). Gene expression was quantified using HTSeq-Counts (v0.6.1) (*48*). Differential expression analysis was performed using DESeq2 (*49*), and subsequent gene set enrichment analysis was performed using the fgsea (*50*) and msigdbr (*51*) R packages, specifically on the Hallmark, KEGG (Kyoto Encyclopedia of Genes and Genomes), and Reactome annotated gene sets. Differentially expressed genes and gene sets were filtered to those with a P value of less than 0.05 and a Benjamini-Hochberg corrected FDR value less than 0.25. Gene expression was visualized using the z score of normalized gene expression (calculated using the variance-stabilizing transform from DESeq2) using the ggplot2 R package (*52*). Gene expression was correlated with the mass cytometry data by calculating the Pearson correlation coefficient between the normalized gene expression (calculated using the variance-stabilizing transform from DESeq2) and the relative percentages of each cell

type (of total CD45$^+$ cells) as determined by cytofkit (described above). Genes most highly correlated with cell types were filtered by those with a Pearson correlation of at least 0.5.

Statistical analysis and reproducibility

Prism (versions 7 and 8) software (GraphPad) was used to analyze differences between groups and determine statistical significance; $P < 0.05$ was considered statistically significant. Normality assumption was evaluated for outcomes before statistical testing. For in vitro studies, including tumor growth, surface protein expression, gene expression, and cytokine production, as well as in vivo tumor growth studies, differences between groups were evaluated using two-sided unpaired *t* tests. For in vivo studies, tumor growth is shown as mean ± SEM. Differences in mouse survival between treatment groups were evaluated using the log-rank test. Statistical analysis of RNA-seq data is described above. Original data are in data file S1.

SUPPLEMENTARY MATERIALS

stm.sciencemag.org/cgi/content/full/12/565/eabb0152/DC1

Fig. S1. Defects in *Jak1* or *Jak2* do not alter sensitivity of irradiated B16 tumors to irradiation and dual ICB.

Fig. S2 CRISPR modifications of B16 tumor cell lines do not alter *gp100* expression.

Fig. S3. MHC I expression of human melanoma exhibits IFN-α dependence.

Fig. S4. MHC I expression of human melanoma exhibits IFN-β dependence.

Fig. S5. Gating strategy to assess in vivo MHC I expression of B16-F10.

Fig. S6. *Nlrc5* overexpression does not augment the antitumor efficacy of adoptively transferred pmel T cells against B16-WT tumors.

Fig. S7. BO-112 augments the efficacy of pmel T cells against B16-WT tumors in vivo.

Fig. S8. BO-112 and pmel ACT alter the immune composition of B16-*Jak1*^{KO} tumors.

Fig. S9. B16-*B2m*^{KO} tumor cells are resistant to killing by pmel T cells.

Fig. S10. BO-112–induced MHC I up-regulation in B16-*Jak1*^{KO} cell lines is *Nlrc5* independent.

Fig. S11. BO-112 induces cytoplasmic phosphorylation and nuclear translocation of NF-κB (p65) in B16-*Jak1*^{KO} cells.

Fig. S12. Protein-level effects of siRNA targeting *Ifih1*, *Ddx58*, or *Tlr3*.

Table S1. CRISPR guides and RT-PCR primer sequences.

Table S2. Reagents.

Data file S1. Original data.

View/request a protocol for this paper from *Bio-protocol*.

REFERENCES AND NOTES

1. D. H. Kaplan, V. Shankaran, A. S. Dighe, E. Stockert, M. Aguet, L. J. Old, R. D. Schreiber, Demonstration of an interferon gamma-dependent tumor surveillance system in immunocompetent mice. *Proc. Natl. Acad. Sci. U.S.A.* **95**, 7556–7561 (1998).
2. A. S. Dighe, E. Richards, L. J. Old, R. D. Schreiber, Enhanced in vivo growth and resistance to rejection of tumor cells expressing dominant negative IFN gamma receptors. *Immunity* **1**, 447–456 (1994).
3. J. M. Zaretsky, A. Garcia-Diaz, D. S. Shin, H. Escuin-Ordinas, W. Hugo, S. Hu-Lieskovan, D. Y. Torrejon, G. Abril-Rodriguez, S. Sandoval, L. Barthly, J. Saco, B. Homet Moreno, R. Mezzadra, B. Chmielowski, K. Ruchalski, I. P. Shintaku, P. J. Sanchez, C. Puig-Saus, G. Cherry, E. Seja, X. Kong, J. Pang, B. Berent-Maoz, B. Comin-Anduix, T. G. Graeber, P. C. Tumeh, T. N.-M. Schumacher, R. S. Lo, A. Ribas, Mutations associated with acquired resistance to PD-1 blockade in melanoma. *N. Engl. J. Med.* **375**, 819–829 (2016).
4. A. Sucker, F. Zhao, N. Pieper, C. Heeke, R. Maltaner, N. Stadtler, B. Real, N. Bielefeld, S. Howe, B. Weide, R. Gutzmer, J. Utikal, C. Loquai, H. Gogas, L. Klein-Hitpass, M. Zeschnigk, A. M. Westendorf, M. Trilling, S. Horn, B. Schilling, D. Schadendorf, K. G. Griewank, A. Paschen, Acquired IFNγ resistance impairs anti-tumor immunity and gives rise to T-cell-resistant melanoma lesions. *Nat. Commun.* **8**, 15440 (2017).
5. S. J. Patel, N. E. Sanjana, R. J. Kishton, A. Eidizadeh, S. K. Vodnala, M. Cam, J. J. Gartner, L. Jia, S. M. Steinberg, T. N. Yamamoto, A. S. Merchant, G. U. Mehta, A. Chichura, O. Shalem, E. Tran, R. Eil, M. Sukumar, E. P. Guijarro, C. P. Day, P. Robbins, S. Feldman, G. Merlino, F. Zhang, N. P. Restifo, Identification of essential genes for cancer immunotherapy. *Nature* **548**, 537–542 (2017).
6. R. T. Manguso, H. W. Pope, M. D. Zimmer, F. D. Brown, K. B. Yates, B. C. Miller, N. B. Collins, K. Bi, M. LaFleur, V. R. Juneja, S. A. Weiss, J. Lo, D. E. Fisher, D. Miao, E. van Allen, D. E. Root, A. H. Sharpe, J. G. Doench, W. N. Haining, In vivo CRISPR screening identifies Ptpn2 as a cancer immunotherapy target. *Nature* **547**, 413–418 (2017).
7. D. Pan, A. Kobayashi, P. Jiang, L. Ferrari de Andrade, R. E. Tay, A. M. Luoma, D. Tsoucas, X. Qiu, K. Lim, P. Rao, H. W. Long, G. C. Yuan, J. Doench, M. Brown, X. S. Liu, K. W. Wucherpfennig, A major chromatin regulator determines resistance of tumor cells to T cell-mediated killing. *Science* **359**, 770–775 (2018).
8. D. S. Shin, J. M. Zaretsky, H. Escuin-Ordinas, A. Garcia-Diaz, S. Hu-Lieskovan, A. Kalbasi, C. S. Grasso, W. Hugo, S. Sandoval, D. Y. Torrejon, N. Palaskas, G. A. Rodriguez, G. Parisi, A. Azhdam, B. Chmielowski, G. Cherry, E. Seja, B. Berent-Maoz, I. P. Shintaku, D. T. le, D. M. Pardoll, L. A. Diaz Jr., P. C. Tumeh, T. G. Graeber, R. S. Lo, B. Comin-Anduix, A. Ribas, Primary resistance to PD-1 blockade mediated by *JAK1/2* mutations. *Cancer Discov.* **7**, 188–201 (2017).
9. A. Kalbasi, A. Ribas, Tumour-intrinsic resistance to immune checkpoint blockade. *Nat. Rev. Immunol.* **20**, 25–39 (2020).
10. I. Voskoboinik, J. C. Whisstock, J. A. Trapani, Perforin and granzymes: Function, dysfunction and human pathology. *Nat. Rev. Immunol.* **15**, 388–400 (2015).
11. T. B. Meissner, A. Li, A. Biswas, K. H. Lee, Y. J. Liu, E. Bayir, D. Iliopoulos, P. J. van den Elsen, K. S. Kobayashi, NLR family member NLRC5 is a transcriptional regulator of MHC class I genes. *Proc. Natl. Acad. Sci. U.S.A.* **107**, 13794–13799 (2010).
12. G. M. Rodriguez, D. Bobbala, D. Serrano, M. Mayhue, A. Champagne, C. Saucier, V. Steimle, T. A. Kufer, A. Menendez, S. Ramanathan, S. Ilangumaran, NLRC5 elicits antitumor immunity by enhancing processing and presentation of tumor antigens to CD8(+) T lymphocytes. *Oncoimmunology* **5**, e1151593 (2016).
13. I. Marquez-Rodas, F. Longo, M. E. Rodriguez-Ruiz, A. Calles, S. Ponce, M. Jove, B. Rubio-Viqueira, J. L. Perez-Gracia, A. Gómez-Rueda, S. López-Tarruella, M. Ponz-Sarvise, R. Álvarez, A. Soria-Rivas, E. de Miguel, R. Ramos-Medina, E. Castañon, P. Gajate, C. Sempere-Ortega, E. Jiménez-Aguilar, M. A. Aznar, A. Calvo, P. P. Lopez-Casas, S. Martín-Algarra, M. Martín, D. Tersago, M. Quintero, I. Melero, Intratumoral nanoplexed poly I:C BO-112 in combination with systemic anti-PD-1 for patients with anti-PD-1 refractory tumors. *Sci. Transl. Med.* **12**, eabb0391 (2020).
14. C. Twyman-Saint Victor, A. J. Rech, A. Maity, R. Rengan, K. E. Pauken, E. Stelekati, J. L. Benci, B. Xu, H. Dada, P. M. Odorizzi, R. S. Herati, K. D. Mansfield, D. Patsch, R. K. Amaravadi, L. M. Schuchter, H. Ishwaran, R. Mick, D. A. Pryma, X. Xu, M. D. Feldman, T. C. Gangadhar, S. M. Hahn, E. J. Wherry, R. H. Vonderheide, A. J. Minn, Radiation and dual checkpoint blockade activate non-redundant immune mechanisms in cancer. *Nature* **520**, 373–377 (2015).
15. J. L. Benci, B. Xu, Y. Qiu, T. J. Wu, H. Dada, C. Twyman-Saint Victor, L. Cucolo, D. S. M. Lee, K. E. Pauken, A. C. Huang, T. C. Gangadhar, R. K. Amaravadi, L. M. Schuchter, M. D. Feldman, H. Ishwaran, R. H. Vonderheide, A. Maity, E. J. Wherry, A. J. Minn, Tumor interferon signaling regulates a multigenic resistance program to immune checkpoint blockade. *Cell* **167**, 1540–1554.e12 (2016).
16. D. P. King, P. P. Jones, Induction of Ia and H-2 antigens on a macrophage cell line by immune interferon. *J. Immunol.* **131**, 315–318 (1983).
17. I. Marquez Rodas, F. Longo, M. Rodriguez-Ruiz, A. Calles, J. L. Pérez-Gracia, A. Gomez-Rueda, S. Lopez-Tarruella, M. Ponz-Sarvisé, R. M. Alvarez, A. Soria, E. de-Miguel, J. Gayarre, M. A. Aznar, A. Calvo, P. P. Lopez-Casas, D. Tersago, M. Quintero, S. Martin-Algarra, M. Martín, I. Melero, Intratumoral BO-112, a double-stranded RNA (dsRNA), alone and in combination with systemic anti-PD-1 in solid tumors. *Ann. Oncol.* **29**, viii732 (2018).
18. H. Häcker, R. M. Vabulas, O. Takeuchi, K. Hoshino, S. Akira, H. Wagner, Immune cell activation by bacterial CpG-DNA through myeloid differentiation marker 88 and tumor necrosis factor receptor-associated factor (TRAF)6. *J. Exp. Med.* **192**, 595–600 (2000).
19. M. C. Bonnet, R. Weil, E. Dam, A. G. Hovanessian, E. F. Meurs, PKR stimulates NF-kappaB irrespective of its kinase function by interacting with the IkappaB kinase complex. *Mol. Cell. Biol.* **20**, 4532–4542 (2000).
20. M. Zamanian-Daryoush, T. H. Mogensen, J. A. DiDonato, B. R. Williams, NF-kappaB activation by double-stranded-RNA-activated protein kinase (PKR) is mediated through NF-kappaB-inducing kinase and IkappaB kinase. *Mol. Cell. Biol.* **20**, 1278–1290 (2000).
21. Z. Jiang, T. W. Mak, G. Sen, X. Li, Toll-like receptor 3-mediated activation of NF-kappaB and IRF3 diverges at Toll-IL-1 receptor domain-containing adapter inducing IFN-beta. *Proc. Natl. Acad. Sci. U.S.A.* **101**, 3533–3538 (2004).
22. J. Gao, L. Z. Shi, H. Zhao, J. Chen, L. Xiong, Q. He, T. Chen, J. Roszik, C. Bernatchez, S. E. Woodman, P. L. Chen, P. Hwu, J. P. Allison, A. Futreal, J. A. Wargo, P. Sharma, Loss of IFN-γ pathway genes in tumor cells as a mechanism of resistance to anti-CTLA-4 therapy. *Cell* **167**, 397–404.e9 (2016).
23. T. Y. Basham, T. C. Merigan, Recombinant interferon-gamma increases HLA-DR synthesis and expression. *J. Immunol.* **130**, 1492–1494 (1983).
24. B. Seliger, U. Wollscheid, F. Momburg, T. Blankenstein, C. Huber, Characterization of the major histocompatibility complex class I deficiencies in B16 melanoma cells. *Cancer Res.* **61**, 1095–1099 (2001).
25. W. W. Overwijk, N. P. Restifo, B16 as a mouse model for human melanoma. *Curr. Protoc. Immunol.* **Chapter 20**, Unit 20.21 (2001).
26. R. Carretero, J. M. Romero, F. Ruiz-Cabello, I. Maleno, F. Rodriguez, F. M. Camacho, L. M. Real, F. Garrido, T. Cabrera, Analysis of HLA class I expression in progressing and regressing metastatic melanoma lesions after immunotherapy. *Immunogenetics* **60**, 439–447 (2008).

27. T. Cabrera, E. Lara, J. M. Romero, I. Maleno, L. M. Real, F. Ruiz-Cabello, P. Valero, F. M. Camacho, F. Garrido, HLA class I expression in metastatic melanoma correlates with tumor development during autologous vaccination. *Cancer Immunol. Immunother.* **56**, 709–717 (2007).
28. E. A. Bach, M. Aguet, R. D. Schreiber, The IFNγ receptor: A paradigm for cytokine receptor signaling. *Annu. Rev. Immunol.* **15**, 563–591 (1997).
29. K. Paucker, K. Cantell, W. Henle, Quantitative studies on viral interference in suspended L cells. III. Effect of interfering viruses and interferon on the growth rate of cells. *Virology* **17**, 324–334 (1962).
30. S. J. Lee, B. C. Jang, S. W. Lee, Y. I. Yang, S. I. Suh, Y. M. Park, S. Oh, J. G. Shin, S. Yao, L. Chen, I. H. Choi, Interferon regulatory factor-1 is prerequisite to the constitutive expression and IFN-gamma-induced upregulation of B7-H1 (CD274). *FEBS Lett.* **580**, 755–762 (2006).
31. A. Garcia-Diaz, D. S. Shin, B. H. Moreno, J. Saco, H. Escuin-Ordinas, G. A. Rodriguez, J. M. Zaretsky, L. Sun, W. Hugo, X. Wang, G. Parisi, C. P. Saus, D. Y. Torrejon, T. G. Graeber, B. Comin-Anduix, S. Hu-Lieskovan, R. Damoiseaux, R. S. Lo, A. Ribas, Interferon receptor signaling pathways regulating PD-L1 and PD-L2 expression. *Cell Rep.* **19**, 1189–1201 (2017).
32. K. E. Cole, C. A. Strick, T. J. Paradis, K. T. Ogborne, M. Loetscher, R. P. Gladue, W. Lin, J. G. Boyd, B. Moser, D. E. Wood, B. G. Sahagan, K. Neote, Interferon-inducible T cell alpha chemoattractant (I-TAC): A novel non-ELR CXC chemokine with potent activity on activated T cells through selective high affinity binding to CXCR3. *J. Exp. Med.* **187**, 2009–2021 (1998).
33. J. M. Farber, A macrophage mRNA selectively induced by gamma-interferon encodes a member of the platelet factor 4 family of cytokines. *Proc. Natl. Acad. Sci. U.S.A.* **87**, 5238–5242 (1990).
34. A. D. Luster, J. C. Unkeless, J. V. Ravetch, Gamma-interferon transcriptionally regulates an early-response gene containing homology to platelet proteins. *Nature* **315**, 672–676 (1985).
35. J. L. Benci, L. R. Johnson, R. Choa, Y. Xu, J. Qiu, Z. Zhou, B. Xu, D. Ye, K. L. Nathanson, C. H. June, E. J. Wherry, N. R. Zhang, H. Ishwaran, M. D. Hellmann, J. D. Wolchok, T. Kambayashi, A. J. Minn, Opposing functions of interferon coordinate adaptive and innate immune responses to cancer immune checkpoint blockade. *Cell* **178**, 933–948.e14 (2019).
36. M. Donia, K. Harbst, M. van Buuren, P. Kvistborg, M. F. Lindberg, R. Andersen, M. Idorn, S. Munir Ahmad, E. Ellebæk, A. Mueller, P. Fagone, F. Nicoletti, M. Libra, M. Lauss, S. R. Hadrup, H. Schmidt, M. H. Andersen, P. thor Straten, J. A. Nilsson, T. N. Schumacher, B. Seliger, G. Jönsson, I. M. Svane, Acquired immune resistance follows complete tumor regression without loss of target antigens or IFNγ signaling. *Cancer Res.* **77**, 4562–4566 (2017).
37. J. Girdlestone, M. Isamat, D. Gewert, C. Milstein, Transcriptional regulation of HLA-A and -B: Differential binding of members of the Rel and IRF families of transcription factors. *Proc. Natl. Acad. Sci. U.S.A.* **90**, 11568–11572 (1993).
38. P. Mansky, W. M. Brown, J. H. Park, J. W. Choi, S. Y. Yang, The second kappa B element, kappa B2, of the HLA-A class I regulatory complex is an essential part of the promoter. *J. Immunol.* **153**, 5082–5090 (1994).
39. M. Forloni, S. Albini, M. Z. Limongi, L. Cifaldi, R. Boldrini, M. R. Nicotra, G. Giannini, P. G. Natali, P. Giacomini, D. Fruci, NF-kappaB, and not MYCN, regulates MHC class I and endoplasmic reticulum aminopeptidases in human neuroblastoma cells. *Cancer Res.* **70**, 916–924 (2010).
40. Y. Cheng, N. J. King, A. M. Kesson, Major histocompatibility complex class I (MHC-I) induction by West Nile virus: Involvement of 2 signaling pathways in MHC-I up-regulation. *J. Infect. Dis.* **189**, 658–668 (2004).
41. S. Heidegger, A. Wintges, F. Stritzke, S. Bek, K. Steiger, P.-A. Koenig, S. Göttert, T. Engleitner, R. Öllinger, T. Nedelko, J. C. Fischer, V. Makarov, C. Winter, R. Rad, M. R. M. van den Brink, J. Ruland, F. Bassermann, T. A. Chan, T. Haas, H. Poeck, RIG-I activation is critical for responsiveness to checkpoint blockade. *Sci. Immunol.* **13**, eaau8943 (2019).
42. J. J. Ishizuka, R. T. Manguso, C. K. Cheruiyot, K. Bi, A. Panda, A. Iracheta-Vellve, B. C. Miller, P. P. Du, K. B. Yates, J. Dubrot, I. Buchumenski, D. E. Comstock, F. D. Brown, A. Ayer, I. C. Kohnle, H. W. Pope, M. D. Zimmer, D. R. Sen, S. K. Lane-Reticker, E. J. Robitschek, G. K. Griffin, N. B. Collins, A. H. Long, J. G. Doench, D. Kozono, E. Y. Levanon, W. N. Haining, Loss of ADAR1 in tumours overcomes resistance to immune checkpoint blockade. *Nature* **565**, 43–48 (2018).
43. F. A. Ran, P. D. Hsu, J. Wright, V. Agarwala, D. A. Scott, F. Zhang, Genome engineering using the CRISPR-Cas9 system. *Nat. Protoc.* **8**, 2281–2308 (2013).
44. M. Haeussler,K. Schönig,H. Eckert,A. Eschstruth,J. Mianné,J. B. Renaud,S. Schneider-Maunoury, A. Shkumatava, L. Teboul, J. Kent, J. S. Joly, J. P. Concordet, Evaluation of off-target and on-target scoring algorithms and integration into the guide RNA selection tool CRISPOR. *Genome Biol.* **17**, 148 (2016).
45. S. C. Wei, J. H. Levine, A. P. Cogdill, Y. Zhao, N. A. A. S. Anang, M. C. Andrews, P. Sharma, J. Wang, J. A. Wargo, D. Pe'er, J. P. Allison, Distinct cellular mechanisms underlie anti-CTLA-4 and anti-PD-1 checkpoint blockade. *Cell* **170**, 1120–1133.e17 (2017).
46. H. Chen, M. C. Lau, M. T. Wong, E. W. Newell, M. Poidinger, J. Chen, Cytofkit: A Bioconductor package for an integrated mass cytometry data analysis pipeline. *PLOS Comput. Biol.* **12**, e1005112 (2016).
47. D. Kim, J. M. Paggi, C. Park, C. Bennett, S. L. Salzberg, Graph-based genome alignment and genotyping with HISAT2 and HISAT-genotype. *Nat. Biotechnol.* **37**, 907–915 (2019).
48. S. Anders, P. T. Pyl, W. Huber, HTSeq—A Python framework to work with high-throughput sequencing data. *Bioinformatics* **31**, 166–169 (2015).
49. M. I. Love, W. Huber, S. Anders, Moderated estimation of fold change and dispersion for RNA-seq data with DESeq2. *Genome Biol.* **15**, 550 (2014).
50. A. A. Sergushichev, An algorithm for fast preranked gene set enrichment analysis using cumulative statistic calculation. bioRxiv 060012 [**Preprint**]. 20 June 2016. https://10.1101/060012.
51. A. Liberzon, C. Birger, H. Thorvaldsdóttir, M. Ghandi, J. P. Mesirov, P. Tamayo, The Molecular Signatures Database (MSigDB) hallmark gene set collection. *Cell Syst.* **1**, 417–425 (2015).
52. H. Wickham, *ggplot2: Elegant Graphics for Data Analysis* (Springer Publishing Company, Incorporated, 2009).

Acknowledgments: We thank W. H. McBride and C. Puig-Saus for scientific discussion and feedback. We acknowledge the UCLA Flow Cytometry Core and the Broad Stem Cell Research Center Flow Cytometry and, in particular, A. Garcia and I. Williams for assistance with flow and mass cytometry and cell sorting, the UCLA Technology Center for Genomics and Bioinformatics for RNA-seq support, and the UCLA Department of Radiation Oncology Mouse Core for assistance with mouse experiments. **Funding:** This study was funded, in part, by the Parker Institute for Cancer Immunotherapy (A.R.); NIH grants R35 CA197633 (A.R.), P01 CA244118 (A.R.), and P01 CA168585 (A.R.); the Ressler Family Fund (A.R.); and the support from Ken and Donna Schultz (A.R.). The study was also supported by UCLA CTSI KL2 Award (NCATS TR001882; A.K.), Sarcoma Alliance for Research Through Collaboration Career Enhancement Program (A.K.), Tower Cancer Research Foundation Young Investigator Award (A.K.), and Radiological Society for North America Research Scholar Grant (A.K.). K.M.C. was supported by the NIH Ruth L. Kirschstein Institutional National Research Service Award #T32-CA009120. R.D.D. was supported by the UCLA Jonsson Comprehensive Cancer Center (JCCC). Flow and mass cytometry were performed in the UCLA JCCC and Center for AIDS Research Flow Cytometry Core Facility that is supported by NIH awards P30 CA016042 and 5P30 AI028697, the UCLA JCCC, the UCLA AIDS Institute, and the David Geffen School of Medicine at UCLA. **Author contributions:** A.K. and A.R. conceived and designed the experiments. A.K., K.H., M.T., S.K., A.V.-C., D.E.S., D.S., J.M.Z., J.M.F., R.D.D., and P.P.L.-C. conducted the experiments and analyzed the data. K.M.C. and A.K. analyzed the RNA-seq data. C.N. conducted blinded tumor measurements. D.T., A.C., and G.P. conducted the experiments. D.E.S. analyzed the data and revised the manuscript. A.K., M.Q., and A.R. wrote and revised the manuscript and supervised the study. **Competing interests:** J.M.F., P.P.L.-C., and M.Q. are employed full-time by Highlight Therapeutics, and M.Q. holds stock. A.R. has received honoraria for consulting with Amgen, Bristol-Myers Squibb, Chugai, Genentech, Merck, Novartis, Roche and Sanofi; is or has been a member of the scientific advisory board; and holds stock in Advaxis, Arcus Biosciences, Highlight Therapeutics, Compugen, CytomX, Five Prime, FLX Bio, ImaginAb, IsoPlexis, Gilead Kite, Lutris Pharma, Merus, PACT Pharma, Rgenix, and Tango Therapeutics. A.K. is a member of the scientific advisory board for T-Cure. A.K. and A.R. are inventors of a patent application covering the therapeutic use of BO-112 in combination with adoptive T cell therapy for cancer ("Methods for treating cancer using adoptive cellular therapy," provisional patent filing number 62/739,783). R.D.D. has consulted for Amgen, Epirium, Holoclara, Acurastem, and Kirkland & Ellis. **Data and materials availability:** All data associated with this study are present in the paper or the Supplementary Materials. BO-112 was obtained through a material transfer agreement with Highlight Therapeutics. Gene expression data (accession numbers GSE157351 and GSE157360) are available at www.ncbi.nlm.nih.gov/geo/.

Submitted 24 January 2020
Accepted 4 September 2020
Published 14 October 2020
10.1126/scitranslmed.abb0152

Citation: A. Kalbasi, M. Tariveranmoshabad, K. Hakimi, S. Kremer, K. M. Campbell, J. M. Funes, A. Vega-Crespo, G. Parisi, A. Champekar, C. Nguyen, D. Torrejon, D. Shin, J. M. Zaretsky, R. D. Damoiseaux, D. E. Speiser, P. P. Lopez-Casas, M. Quintero, A. Ribas, Uncoupling interferon signaling and antigen presentation to overcome immunotherapy resistance due to JAK1 loss in melanoma. *Sci. Transl. Med.* **12**, eabb0152 (2020).

Science Translational Medicine

Uncoupling interferon signaling and antigen presentation to overcome immunotherapy resistance due to JAK1 loss in melanoma

Anusha Kalbasi, Mito Tariveranmoshabad, Kevin Hakimi, Sarah Kremer, Katie M. Campbell, Juan M. Funes, Agustin Vega-Crespo, Giulia Parisi, Ameya Champekar, Christine Nguyen, Davis Torrejon, Daniel Shin, Jesse M. Zaretsky, Robert D. Damoiseaux, Daniel E. Speiser, Pedro P. Lopez-Casas, Marisol Quintero and Antoni Ribas

Sci Transl Med **12**, eabb0152.
DOI: 10.1126/scitranslmed.abb0152

Interfering with cancer

Many immunotherapies for cancer have emerged in recent years, but none are universally effective. One potential problem is the loss of interferon signaling in tumors, which impairs the effectiveness of both immune checkpoint blockade and cell-based therapies. Kalbasi *et al.* determined that both JAK1 and JAK2 signaling were essential for the success of immune checkpoint blockade, whereas cell-based therapy only required JAK1 function, which maintained sufficient interferon signaling. The authors showed that defective interferon signaling in tumors could be bypassed with the immunostimulatory compound BO-112. In a companion clinical trial, Márquez-Rodas *et al.* tested BO-112 in human patients with cancer, with or without immune checkpoint blockade.

Science Translational Medicine (ISSN 1946-6242) is published by the American Association for the Advancement of Science, 1200 New York Avenue NW, Washington, DC 20005. The title *Science Translational Medicine* is a registered trademark of AAAS.